Modeling and Compensation of Nonlinear Distortion in Multi-Antenna RF Transmitters

KATHARINA HAUSMAIR

Modeling and Compensation of Nonlinear Distortion in Multi-Antenna RF Transmitters

Katharina Hausmair

Division of Communication and Antenna Systems
Department of Electrical Engineering
Chalmers University of Technology
SE-412 96 Göteborg, Sweden
Phone: +46 (0) 31 772 1000
Email: hausmair@chalmers.se; hausmair@gmail.com

Abstract

Multi-antenna systems are utilized as a way to increase spectral efficiency in wireless communications. In a transmitter, the use of several parallel transmit paths and antennas increases system complexity and cost. Cost-efficient solutions, which employ active antenna arrays and avoid expensive isolators, are therefore preferred. However, such solutions are vulnerable to crosstalk due to mutual coupling between the antennas, and impedance mismatches between amplifiers and antennas. Combined with the nonlinear behavior of the power amplifiers, these effects cause nonlinear distortion, which deteriorates the quality of the transmitted signals and can prevent the transmitter from meeting standard requirements and fulfilling spectrum regulations. Analysis, assessment and, if necessary, compensation of nonlinear distortion are therefore essential for the design of multi-antenna transmitters.

In this thesis, a technique for modeling and predicting nonlinear distortion in multi-antenna transmitters is presented. With this technique, the output of every individual transmit path, as well as the radiated far-field of the transmitter can be predicted with low computational effort. The technique connects models of the individually characterized transmitter components. It can be used to investigate and compare the effects of different power amplifier and antenna array designs at early design stages without complicated and expensive measurements.

Furthermore, a digital predistortion technique for compensating nonlinear distortion in multi-antenna transmitters is presented. Digital predistortion is commonly used in transmitters to compensate for undesired nonlinear hardware effects. The proposed solution combines a linear function block with dual-input predistorters. The complexity is reduced compared to existing techniques, which require highly complex multivariate predistorter functions.

Finally, a technique for identifying multi-antenna transmitter models and predistorters from over-the-air measurements using only a small set of observation receivers is presented. Conventional techniques require a dedicated observation receiver in every transmitter path, or one or more observation receivers that are shared by several paths in a time-interleaved manner. With the proposed technique, each receiver is used to observe several transmitter paths simultaneously. Compared to conventional techniques, hardware cost

and complexity can be reduced with this approach.

In summary, the signal processing techniques presented in this thesis enable a simplified, low-cost design process of multi-antenna transmitters. The proposed algorithms allow for feasible, low-complexity implementations of both digital and analog hardware even for systems with many antennas, thereby facilitating the development of future generations of wireless communication systems.

Keywords: antenna crosstalk, behavioral modeling, digital predistortion, linearization, multi-antenna transmitter, over-the-air characterization, power amplifier.

Acknowledgments

I would like to thank everyone who has supported me in writing this thesis.

First, I would like to thank my team of supervisors. Thomas Eriksson, thank you for encouraging me with your continuous optimism every time I felt that my work was not going anywhere. Christian Fager, thank you for all the discussions and your unfailing support, it was great to have your reliable guidance all these years. Ulf Gustavsson, thank you for helping me out in the lab many times, without you many of my results would not have been possible. Per N. Landin, thanks for always being there to discuss things with me, even after you left Chalmers.

I also want to thank all my colleagues at E2 and MC2 for the great work environment. Thanks also to the administrative staff at E2, especially Agneta Kinnander and Lars Börjesson. To my office mate Jessica Chani-Cahuana, I am glad I had you to share this experience with. Special thanks goes to Sebastian Gustafsson, thank you for all the time you spent patiently introducing me to the world of RF measurements.

I also want to say thanks my friends and family. Thank you for your continuous support in all my endeavors. To Víctor, thank you for motivating me to get through this, and for always being there for me.

List of Publications

Appended Publications

This thesis is based on the following papers.

[A] **K. Hausmair**, S. Gustafsson, C. Sánchez-Pérez, P. N. Landin, U. Gustavsson, T. Eriksson, and C. Fager "Prediction of Nonlinear Distortion in Wideband Active Antenna Arrays", in *IEEE Transactions on Microwave Theory and Techniques*, vol. 65, no. 11, pp. 4550-4563, Nov 2017, `https://doi.org/10.1109/TMTT.2017.2699962`.

[B] **K. Hausmair**, P. N. Landin, U. Gustavsson, C. Fager, and T. Eriksson, "Digital Predistortion for Multi-Antenna Transmitters Affected by Antenna Crosstalk", in *IEEE Transactions on Microwave Theory and Techniques*, awaiting publication (accepted in August 2017), `https://doi.org/10.1109/TMTT.2017.2748948`.

[C] **K. Hausmair**, U. Gustavsson, C. Fager, and T. Eriksson, "Over-the-Air Linearization of Multi-Antenna Transmitters Affected by Antenna Crosstalk", to be submitted to *IEEE Transactions on Communications*.

Other Publications

The following publications are not included in the thesis because the content partially overlaps with the appended papers, or the content is out of the scope of this thesis.

Papers

[a] C. Vogel, M. Hotz, S. Saleem, **K. Hausmair** and M. Soudan, "A Review on Low-Complexity Structures and Algorithms for the Correction of Mismatch Errors in Time-Interleaved ADCs," *IEEE International New Circuits and Systems Conference*, Montreal, 2012, pp. 349-352.

[b] **K. Hausmair**, S. Chi, P. Singerl and C. Vogel, "Aliasing-Free Digital Pulse-Width Modulation for Burst-Mode RF Transmitters," in *IEEE Transactions on Circuits and Systems I: Regular Papers*, vol. 60, no. 2, pp. 415-427, Feb 2013.

[c] **K. Hausmair**, P. Singerl and C. Vogel, "Multiplierless Implementation of an Aliasing-Free Digital Pulsewidth Modulator," in *IEEE Transactions on Circuits and Systems II: Express Briefs*, vol. 60, no. 9, pp. 592-596, Sep 2013.

[d] **K. Hausmair**, S. Chi and C. Vogel, "How to Reach 100% Coding Efficiency in Multilevel Burst-Mode RF Transmitters," *IEEE International Symposium on Circuits and Systems*, Beijing, 2013, pp. 2255-2258.

[e] S. Chi, **K. Hausmair** and C. Vogel, "Coding Efficiency of Bandlimited PWM Based Burst-Mode RF Transmitters," *IEEE International Symposium on Circuits and Systems*, Beijing, 2013, pp. 2263-2266.

[f] U. Gustavsson, C. Sánchez-Pérez, T. Eriksson, F. Athley, G. Durisi, P. Landin, **K. Hausmair**, C. Fager, L. Svensson, "On the Impact of Hardware Impairments on Massive MIMO," *IEEE Globecom Workshops*, Austin, TX, 2014, pp. 294-300.

[g] C. Fager, X. Bland, **K. Hausmair**, J. Chani-Cahuana and T. Eriksson, "Prediction of Smart Antenna Transmitter Characteristics Using a New Behavioral Modeling Approach," *IEEE International Microwave Symposium*, Tampa, FL, 2014, pp. 1-4.

[h] C. Fager, **K. Hausmair**, T. Eriksson and K. Buisman, "Analysis of Thermal Effects in Active Antenna Array Transmitters Using a Combined EM/Circuit/Thermal Simulation Technique," *Integrated Nonlinear Microwave and Millimetre-wave Circuits Workshop*, Taormina, 2015, pp. 1-3.

[i] C. Fager, **K. Hausmair**, K. Buisman, K. Andersson, E. Sienkiewicz and D. Gustafsson, "Analysis of Nonlinear Distortion in Phased Array Transmitters," *Integrated Nonlinear Microwave and Millimetre-wave Circuits Workshop*, Graz, 2017, pp. 1-4.

[j] **K. Hausmair**, U. Gustavsson, C. Fager, T. Eriksson, "Modeling and Linearization of Multi-Antenna Transmitters Using Over-the-Air Measurements," accepted for presentation at *IEEE International Symposium on Circuits and Systems*, Florence, 2017.

Patent Applications

[k] **K. Hausmair**, T. Eriksson, U. Gustavsson and C. Fager, "Apparatus and Method for Identification and Compensation of Distortion in a Multi-Antenna System," *Patent Application (WO2017198288)*, published Nov 23, 2017.

[l] U. Gustavsson, P. N. Landin, **K. Hausmair** and T. Eriksson, "An Antenna Arrangement for Non-Linear Distortion Mitigation," *Patent Application (WO2016045724)*, published March 31, 2016.

Contents

Acronyms

ACEPR	Adjacent Channel Error Power Ratio
ACLR	Adjacent Channel Leakage Ratio
ACPR	Adjacent Channel Power Ratio
AWGN	Additive White Gaussian Noise
CTMM	Crosstalk And Mismatch Model
DLA	Direct Learning Architecture
DPD	Digital Predistortion
FIR	Finite Impulse Response
ILA	Indirect Learning Architecture
ILC	Iterative Learning Control
IQ	In-Phase/Quadrature
MILA	Model-Based Indirect Learning Architecture
MIMO	Multiple-Input Multiple-Output
NMSE	Normalized Mean Square Error
OFDM	Orthogonal Frequency Division Multiplexing
PA	Power Amplifier
PAPR	Peak-to-Average Power Ratio
PHD	Polyharmonic Distortion
PSD	Power Spectral Density
QAM	Quadrature Amplitude Modulation
RF	Radio Frequency
SNR	Signal-to-Noise Ratio
VNA	Vector Network Analyzer

Part I

Overview

Chapter 1

Introduction

To cope with the ever-increasing demand for high data rates, making efficient use of the limited radio spectrum is imperative [1]. Wireless communication systems utilize spectrally efficient modulation schemes, like high-order quadrature amplitude modulation (QAM) in combination with orthogonal frequency division multiplexing (OFDM), to combat the limitation of the precious resource [2]. To further expand the capacity of wireless networks, multi-antenna systems, often referred to as multiple-input multiple-output (MIMO) systems, are employed in modern and future telecommunication standards [3]. Attempting to keep system complexity and cost low, integrated radio frequency (RF) transmitter designs employing active antennas are used, where expensive and bulky components like isolators between power amplifiers (PAs) and antennas are avoided [4].

Due to the large peak-to-average power ratios (PAPRs) of the transmission signals of modern wireless communication systems, imperfections of the transmitter hardware, like nonlinear PA characteristics, result in nonlinear distortion [5, 6]. In addition to that, integrated multi-antenna systems are also vulnerable to antenna crosstalk due to mutual coupling and impedance mismatches [7], which causes even more nonlinear distortion. Nonlinear distortion impacts not just the transmission of the respective user, but can also compromise transmissions in neighboring frequency bands, since power is leaked into parts of the frequency spectrum assigned to other users. Hence, in order to maintain system integrity and avoid violating tight spectrum regulations and communication standard requirements, compensation techniques are needed to mitigate nonlinear distortion at the transmitter.

Modeling and analysis of nonlinear PA distortion in RF transmitters and the development of suitable techniques, like digital predistortion (DPD), to compensate for it have been important topics in research for many years [8, 9, 10]. Since the trend for larger scale multi-antenna systems, such as massive MIMO [11], is rather recent, most available solutions do not consider the effects of antenna crosstalk. Therefore, it is necessary to extend and complement

existing approaches in order to deal with these challenges [12].

In this thesis, a technique for modeling and predicting the output of multi-antenna RF transmitters suffering from PA nonlinearities, antenna crosstalk and mismatch is presented. Different alternatives for model identification are proposed. Since implementing and measuring multi-antenna systems is complicated and expensive, low complexity and feasibility were taken into consideration when proposing the model identification procedures. Furthermore, a compensation technique is proposed that can eliminate the joint nonlinear effects of PA, antenna crosstalk and mismatch. Again, complexity was a major concern in order to make the technique suitable for a system implementation.

1.1   Thesis Outline

The remainder of this thesis is organized as follows: Chapter 2 serves as an introduction to modeling and linearization of RF transmitters. The problem of nonlinear distortion due to imperfections in the transmitter hardware is explained. Common techniques for behavioral modeling of PA distortion, as well as DPD as a technique for linearization are introduced. Chapter 3, presents the challenges faced in multi-antenna transmitters, where in addition to PA distortion nonlinear effects due to different types of crosstalk are present. Different system models are discussed, and a review of existing modeling and linearization approaches is given to clearly define the contribution of the work proposed in this thesis. In Chapter 4, a new approach to model and predict the behavior of multi-antenna transmitters suffering from antenna crosstalk is presented and compared to existing approaches. Different methods to identify model coefficients are presented. A low-complexity DPD technique suitable for compensating nonlinear distortion due to PA nonlinearities and antenna crosstalk is presented in Chapter 5. Chapter 6 concludes the thesis by giving a summary of the contributions of the presented work and discussing possible research topics for future work.

Chapter 2

Background

RF transmitters suffer from nonlinear distortion due to hardware imperfections. If no distortion compensation is used, the transmitted signal deviates from the desired transmit signal. Figure 2.1a shows an example of how nonlinear distortion affects the amplitude of the transmitted signal by comparing it to the amplitude of an ideal transmit signal. One consequence of this deterioration of transmit signal quality is an increased amount of errors in the receiver, which decreases the throughput of the communication system. Perhaps the most severe consequence of nonlinear distortion is that it leads to spectral regrowth, which means that power is leaked into neighboring frequency bands. This is illustrated in Figure 2.1b. To avoid interference between transmissions, stringent spectrum regulations only allow small amounts of leakage into adjacent channels. Transmit signals that violate these spectrum regulations must not be transmitted. Hence, nonlinear distortion has to be compensated for at the transmit side the communication system.

Understanding the cause and behavior of nonlinear distortion, predicting its effects, as well as finding adequate linearization techniques to compensate for these effects, have been important topics in research for many years. Many approaches and techniques have been proposed for modeling and linearization of typical wireless single-antenna transmitters [13]. While, in general, these techniques are not sufficient to model and linearize multi-antenna transmitters, similar basic concepts and ideas can be used. In this chapter, the basic techniques and concepts that have been applied or adapted for the work in this thesis are introduced.

2.1 Modeling Nonlinear Distortion in RF Transmitters

The aim of modeling RF transmitters is to find a suitable description of the behavior of the RF transmitter. The model can then be used to predict the
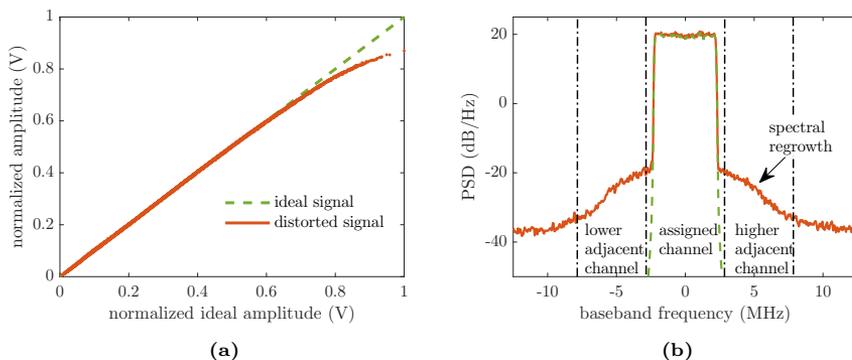
Figure 2.1. The effects of nonlinear distortion due to transmitter hardware imperfections. In (a), effects on the amplitude of a transmit signal are shown, where it is clearly visible that the distorted signal deviates from the ideal linear curve. In (b), the power spectral densities (PSDs) of distorted signal and desired signal are shown to illustrate the problem of spectral regrowth leaking into adjacent channels.

output of the transmitter for a specific input signal. Hence, models help to analyze the performance of transmitters, and they can be used to test algorithms offline, which helps avoid expensive and complicated measurement campaigns. Furthermore, the knowledge obtained from modeling a transmitter is often used as a basis for the development of linearization techniques.

The RF transmitter in a traditional wireless communication system has one transmit path that uses many individual hardware components. Figure 2.2 shows the main components of an RF transmitter chain in a simplified block diagram. All hardware components cause certain impairments that deteriorate the performance of the transmitter, such as in-phase/quadrature (IQ) imbalance, quantization noise, phase noise, etc. The main source of nonlinear distortion in the transmitter is the PA. Therefore, modeling nonlinear distortion in typical RF transmitters is often considered equivalent to modeling the nonlinear distortion introduced by the PA, and it is common to use an even more simplified system model, which is shown in Figure 2.3.

In addition to nonlinear distortion, PAs often cause dynamic distortion, i.e., the output of the PA depends not only on the current value of the input signal, but also on past values [14]. Dynamic distortion occurs when the input signal to the PA is wider than the bandwidth over which the PA is affecting all frequencies in the same way. This behavior is often referred to as memory effects, and it has to be considered in modeling as well.

As is commonly done in transmitter modeling, the system model of the transmitter is given in the equivalent discrete-time low-pass description [15].
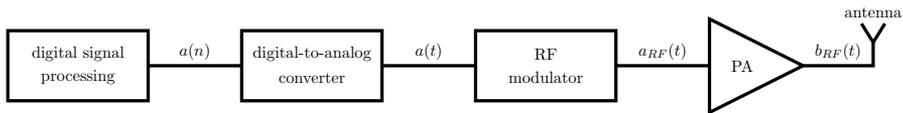
Figure 2.2. Block diagram of a typical RF transmitter chain, showing the main hardware components, i.e., digital signal processing unit, digital-to-analog converter, RF modulator, and PA.
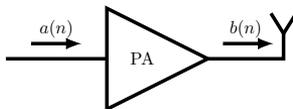
Figure 2.3. Block diagram of the system model of an RF transmitter for the purpose of modeling and digital predistortion.

The output $b(n)$ of the PA is described as a function of the input $a(n)$ as [1]

$$b(n) = f(a(n)). \tag{2.1}$$

2.1.1 Model Structures

The function $f(a(n))$ that can adequately characterize the behavior of the system is what is referred to as the model of the transmitter. Many different types of functions have been proposed for modeling different types of transmitters, and finding suitable so-called model structures has been an important research topic [16]. The Volterra series and reduced versions thereof are among the most popular model structures [17]. A Volterra series model is given by [18]

$$b(n) = \sum_{m_1=0}^{M} \theta_{0m_1} a(n - m_1) + \sum_{p=1}^{(P-1)/2} \Bigg[$$

$$\sum_{m_1=0}^{M} \cdots \sum_{m_{p+1}=m_p}^{M} \sum_{m_{p+2}=0}^{M} \cdots \sum_{m_{2p+1}=m_{2p}}^{M} \theta_{pm_1,m_2,\ldots,m_{2p+1}}$$

$$\times \prod_{k=1}^{p+1} a(n - m_k) \prod_{l=p+2}^{2p+1} a^*(n - m_l) \Bigg] \tag{2.2}$$

where θ are complex coefficients, P is the nonlinear order, M is the memory depth and $(\cdot)^*$ denotes the complex conjugate. Only odd order combinations of the input signal $a(n)$ are considered in the model, where each combination contains exactly one less conjugate term than non-conjugate terms. This is

---

[1]Strictly speaking, (2.1) should be written as $b(n) = f(a(n), a(n-1), a(n-2), \ldots)$ to account for dependency of $b(n)$ on current and past samples of the input signals $a(n)$. However, readability is favored over strict mathematical soundness here and for equations of the same nature in the rest of the thesis.

because only these combinations result in signal components located in the frequency band that is relevant to the description of the nonlinear system [19]. As can be seen, the model structure is the sum of different combinations of the input signal $a(n)$, called basis functions, weighted by the complex coefficients θ. Therefore, the model in (2.2) can be written as

$$b(n) = \mathbf{G}\left(a(n)\right)\boldsymbol{\theta} \tag{2.3}$$

where $\mathbf{G}\left(a(n)\right)$ is a matrix containing the basis functions, i.e.,

$$\mathbf{G}\left(a(n)\right) = \begin{bmatrix} a(n) & a(n-m_1) & \cdots & a(n)|a(n)|^2 & a(n)|a(n)|^4 & \cdots \end{bmatrix} \tag{2.4}$$

where $|\cdot|$ denotes the absolute value. The vector $\boldsymbol{\theta} = [\theta_{00}, \theta_{01}, \ldots, \theta_{10}, \theta_{20}, \ldots]^T$ contains the complex coefficients, where $(\cdot)^T$ denotes the matrix transpose.

Since a model based on the full Volterra series is very complex, many model structures have been proposed to reduce the number of basis functions and model coefficients [20], for example, polynomial, memory polynomial [14], generalized memory polynomial [19], etc. For the work presented in this thesis, the polynomial and memory polynomial and structures related to these have been used. The polynomial, which is suitable for PAs without dynamic behavior, is given by

$$b(n) = \sum_{p=0}^{(P-1)/2} \theta_p a(n)|a(n)|^{2p}. \tag{2.5}$$

The memory polynomial, which is capable of describing dynamic behavior, is given by [14]

$$b(n) = \sum_{p=0}^{(P-1)/2} \sum_{m=0}^{M} \theta_{pm} a(n-m)|a(n-m)|^{2p}. \tag{2.6}$$

Both the polynomial model and memory polynomial model, as well as other pruned-Volterra series models, can be expressed by (2.3).

2.1.2 Identification of Model Coefficients

Once a suitable model structure has been found, the model coefficients in $\boldsymbol{\theta}$ have to be identified. This can be done by measuring a number of samples N of the output of the system for a known input signal, such that

$$\mathbf{b} = \mathbf{G}\left(\mathbf{a}\right)\boldsymbol{\theta} \tag{2.7}$$

where $\mathbf{b} = [b(0), \ldots, b(N-1)]^T$ and $\mathbf{a} = [a(0), \ldots, a(N-1)]^T$. The linear least-squares solution for the model coefficients $\boldsymbol{\theta}_{LS}$ is given by

$$\boldsymbol{\theta}_{LS} = \mathbf{G}\left(\mathbf{a}\right)^{+}\mathbf{b} \tag{2.8}$$

where the Moore-Penrose pseudoinverse $\mathbf{X}^{+} = (\mathbf{X}^H\mathbf{X})^{-1}\mathbf{X}^H$ is used, with $(\cdot)^H$ denoting the Hermitian transpose and $(\cdot)^{-1}$ denoting the matrix inverse.

2.1.3   Model Evaluation

In order to evaluate the accuracy of a model, several performance metrics can be calculated. Among the most common are the normalized mean square error (NMSE) and the adjacent channel error power ratio (ACEPR) [20]. The NMSE is used as a measure for model performance at in-band frequencies, while the ACEPR is a measure for how well the model performs in neighboring channels [21]. The NMSE between the model output $\tilde{b}(n)$ and the measured data $b(n)$ is calculated as

$$\text{NMSE} = \frac{\sum_{n=0}^{N-1} |b(n) - \tilde{b}(n)|^2}{\sum_{n=0}^{N-1} |b(n)|^2}. \tag{2.9}$$

The ACEPR is calculated as

$$\text{ACEPR} = \max_{c=1,2} \left\{ \frac{\sum_{f_{(adj)_c}} |B(f) - \tilde{B}(f)|^2}{\sum_{f_{ch}} |B(f)|^2} \right\} \tag{2.10}$$

where $\tilde{B}(f)$ and $B(f)$ are the Fourier transforms of the model output and the measured data, f_{ch} denotes inband frequencies, $f_{(adj)_1}$ the frequencies in the lower adjacent channel, and $f_{(adj)_2}$ the frequencies in the upper adjacent channel. Hence, the ACEPR is calculated for both the upper and the lower adjacent channels, with the maximum used for evaluation.

2.2   Digital Predistortion

DPD is a technique used to pre-compensate for undesired nonlinear and dynamic behavior. A basic block diagram of an RF transmitter with DPD is shown in Figure 2.4. The goal of DPD is to make the overall system linear, such that the actual transmit signal $b(n)$ is equal to a desired transmit signal $b_d(n)$. The predistorter calculates an input signal to the PA that is meant to achieve this goal. This predistorted signal $a(n)$ is given as a function of the desired signal $b_d(n)$ by

$$a(n) = \hat{f}\left(b_d(n)\right). \tag{2.11}$$

The predistorter function $\hat{f}\left(b_d(n)\right)$ that achieves linearization has to be determined. Finding a suitable structure for the predistorter is often based on modeling results and has been an equally important topic in research. The most common choice is using a structure that performs well for modeling of the same system, even though alternative ways of finding predistorter structures have been proposed, e.g., [16]. Hence, similar to PA modeling, Volterra series-based structures have been used for DPD. The predistorted signal can be written as

$$a(n) = \hat{\mathbf{G}}\left(b_d(n)\right)\hat{\boldsymbol{\theta}} \tag{2.12}$$
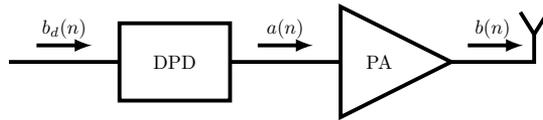
Figure 2.4. Block diagram of an RF transmitter with DPD.

where $\hat{\mathbf{G}}\left(b_d(n)\right)$ contains the predistorter basis functions and $\hat{\boldsymbol{\theta}}$ contains the predistorter coefficients. For a sequence of N samples this is expressed as

$$\mathbf{a} = \hat{\mathbf{G}}\left(\mathbf{b}_d\right)\hat{\boldsymbol{\theta}} \qquad (2.13)$$

where $\mathbf{b}_d = [b_d(0),\ldots,b_d(N-1)]^T$.

2.2.1 Identification of DPD Coefficients

Different approaches have been proposed for identification of the DPD coefficients, for example, direct learning architecture (DLA) [22], indirect learning architecture (ILA) [23], model-based ILA (MILA) [24], and iterative learning control (ILC) [25]. In general, all approaches require the measurement of the PA output signal $b(n)$ while applying a known input signal $a(n)$. In practice, these measurements are done with a dedicated observation receiver that utilizes a coupler and a full receiver chain to measure the PA output signal $b(n)$ [26].

For the work presented in this thesis, the ILA approach in [27] and MILA have been used. Hence, only these two techniques are described here. The idea behind ILA is to find a post-inverse function of the PA behavior and use it as a pre-inverse in the predistorter. A block diagram of a transmitter using DPD based on ILA is shown in Figure 2.5. The post-inverse is the function that, when applied to the output $b(n)$ of a PA driven with $a(n)$, has the signal $a(n)$ as output, i.e.,

$$a(n) = \hat{\mathbf{G}}\left(b(n)\right)\hat{\boldsymbol{\theta}}. \qquad (2.14)$$

Hence, the least squares-solution of the coefficients $\hat{\boldsymbol{\theta}}_{LS}$ for the ILA-based predistorter is given by

$$\hat{\boldsymbol{\theta}}_{LS} = \hat{\mathbf{G}}\left(\mathbf{b}\right)^{+}\mathbf{a}. \qquad (2.15)$$

When using ILA, noise results in a biased estimate of the model coefficients [28]. MILA solves this problem by first finding a PA model based on measurements, and then using the PA model output rather than the measured PA output to identify the predistorter [24].

2.2.2 Evaluation of DPD Performance

Similar as in modeling, the NMSE is also used for the evaluation of in-band DPD performance. The NMSE used for DPD evaluation is calculated between
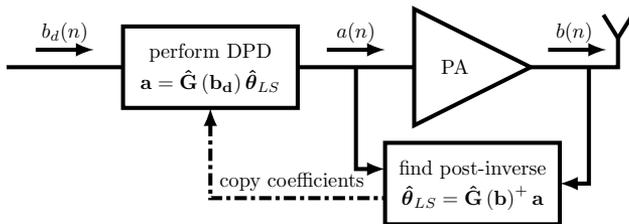
Figure 2.5. Block diagram of an RF transmitter with DPD based on ILA, where a post-inverse of the PA function is used as a predistorter.

the measured PA output $b(n)$ and the desired signal $b_d(n)$ as

$$\text{NMSE} = \frac{\sum_{n=0}^{N-1}|b_d(n) - b(n)|^2}{\sum_{n=0}^{N-1}|b_d(n)|^2}. \quad (2.16)$$

The adjacent channel power ratio (ACPR), also referred to as adjacent channel leakage ratio (ACLR), is used as a measure for how well distortion in neighboring channels is compensated for. The ACPR is calculated by

$$\text{ACPR} = \max_{c=1,2} \left\{ \frac{\sum_{f_{(adj)_c}}|B(f)|^2}{\sum_{f_{ch}}|B(f)|^2} \right\}. \quad (2.17)$$

2.2.3 Complexity

In order to make DPD feasible for a system implementation, it is important to keep the complexity low. Different types of complexity have to be considered [29]:

- Run-time complexity is the complexity to calculate the predistorted signal. It depends on the number of calculations that are required for each input signal sample, and on the sampling rate of the system. The number of calculations per sample depends on the number of predistorter coefficients.

- Identification complexity is the complexity required to find an initial version of the predistorter coefficients. Typically, this is done in the lab or factory using least-squares techniques [30]. Therefore, identification complexity is often considered negligible.

- Adaptation complexity is the complexity to adjust the predistorter coefficients to changes in system behavior during runtime. Algorithms like least mean squares, recursive least squares, or similar [31] can be used for adaptation. Adaptation complexity depends on the number of coefficients that need to be updated, and on how much and how fast the systems changes over time.

Exact complexity measures, such as power consumption, cost, and space, always depend on a specific implementation, i.e., implementation concept [31, 32, 33], used hardware, necessity and frequency of adaptation, training algorithm, adaptation algorithm, bandwidth requirements etc. However, all types of complexity scale with the number of required DPD coefficients. Therefore, when considering Volterra series-based DPD structures that have the same requirements for sampling rate, complexity comparison of different predistorters is commonly based on comparing the number of DPD coefficients. Reducing the number of coefficients is often used as a technique to reduce complexity [13, 34, 35, 36, 37].

Note that complexity is usually not an issue for modeling. Modeling is normally performed in the lab or factory for analysis and testing, but is not part of the running system. However, when using model-based DPD identification techniques, complexity of the PA model structure could become important as well.

2.3   Notation

Throughout this thesis, letters of the Greek alphabet are used for complex coefficients. The letters a and b always stand for signals. Bold letters in lower case indicate vectors, and bold letters in upper case matrices.

For the remainder of this thesis, a slightly different variable notation than in this chapter will be used in order to improve the legibility of equations: where applicable and if not explicitly stated otherwise, time dependency is omitted for better legibility, such that for example $a(n)$ is written as a, $f(a(n))$ as $f(a)$, etc.

Chapter 3

Multi-Antenna RF Transmitters - Introduction and Review

In this chapter, first the challenges for modeling and linearization of multi-antenna transmitters are explained. Then, system models of multi-antenna transmitters suffering from different types of impairments are described. It is explained, which issues have already been addressed in literature, and which issues have been investigated for the work presented in this thesis. Hence, in this chapter, the contribution of this thesis in relation to other published work is defined. Details about the proposed solutions and results are addressed later on in Chapters 4 and 5.

3.1   Challenges

The multi-antenna transmitters considered in this thesis are making use of several transmit paths in parallel, working on the same center frequency. Each transmit path is a fully equipped transmitter chain with its own PA and antenna. Together, the antennas of all transmit paths form an active antenna array. A block diagram of a multi-antenna RF transmitter with K paths is shown in Figure 3.1. Implementing a transmitter with several parallel paths poses challenges not only from a hardware design perspective, but also from a signal processing point of view. This is because such transmitters are vulnerable to undesired hardware effects that are not present in conventional single-path transmitters, and cannot be dealt with by conventional modeling and compensation techniques.

Employing several transmit paths obviously results in an increase of system complexity and cost. The complexity and feasibility of analog and digital
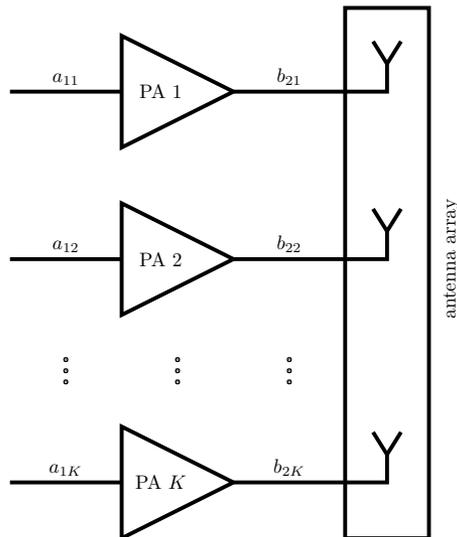
Figure 3.1. Block diagram of a multi-antenna RF transmitter with K parallel transmit paths.

hardware solutions is therefore a major concern in the design of multi-antenna systems. When it comes to the analog hardware, it is often preferred to use active antenna system designs. To aim for low-cost designs, bulky and expensive hardware components like isolators between PAs and antennas are avoided [7]. Such isolators were usually employed to prevent that the PA output signals mix with antenna crosstalk and mismatch. Other multi-antenna system designs choose to integrate multiple transmit paths on the same chipset, sharing the hardware of the local oscillator [38, 39]. As a consequence, multi-antenna transmitter designs can suffer from different types of crosstalk and mismatch. Crosstalk is interference between the different transmit paths, which can result in undesired linear and nonlinear distortion in the transmitter output signals. All types of crosstalk effects have in common that they cannot simply be modeled or linearized using PA model structures and predistorter structures designed for conventional single-path systems. Hence, model and predistorter structures have to be found that can adequately describe these effects. Especially for predistorter structures, it is important to consider the computational complexity at run-time in order to make their use in a system implementation feasible.

Modeling an RF transmitter usually requires the knowledge of input and output signals of the system, which means that the transmitter has to be implemented to some extent in order to perform the measurements which are used for model extraction. To save the time and cost of completely redesigning the system, techniques are desired that can predict the performance of a multi-

antenna transmitter at an early design stage.

Another challenge with multi-antenna transmitters is that it is cumbersome to perform the measurements that are necessary to analyze, model and linearize them even when the system has been fully implemented. Performing well-synchronized measurements of the output signals of several transmit paths can be difficult or even impossible depending on the specific hardware design or laboratory equipment. For performance evaluation, the radiated transmit signals have to be analyzed as well, which requires over-the-air measurements. For predistortion, it is necessary to track changes in system behavior once the system is operating. However, implementing an observation receiver in every transmit path would cause a drastic increase in hardware complexity. It is therefore important to find feasible techniques to measure and identify the information necessary for analysis, modeling and predistortion of multi-antenna transmitters.

3.2 Multi-Antenna RF Transmitter System Models

Like conventional single-path transmitters, multi-antenna transmitters suffer from nonlinear distortion due to the PA. In addition to the PA distortion, crosstalk effects can be present as well. These effects need to be considered in the system model. Different system designs suffer from different types of crosstalk. Crosstalk can therefore be categorized into several types, all of which can be described by dedicated system models. There are three main types of crosstalk: crosstalk that is introduced before the PAs, crosstalk that is introduced after the amplification stages and is purely additive, and antenna crosstalk in combination with mismatch.

3.2.1 Systems Without Crosstalk

The system model of a multi-antenna transmitter suffering from no other distortion than the nonlinear behavior of the PA is given by

$$b_{2k} = f_k\left(a_{1k}\right) \tag{3.1}$$

where $f_k(\cdot)$ describes the behavior of the kth PA, a_{1k} is the input to the kth transmit path and b_{2k} its output. The output of the kth transmit path depends only on the input to the same path, exactly as in a conventional single-path transmitter in (2.1). Therefore, conventional PA model structures and predistorters can be used for modeling and linearizing such transmitters.

3.2.2 Crosstalk Before the Power Amplifiers

For system designs on a single chipset, interference between the different transmit paths can be introduced due to electromagnetic coupling and leakage of
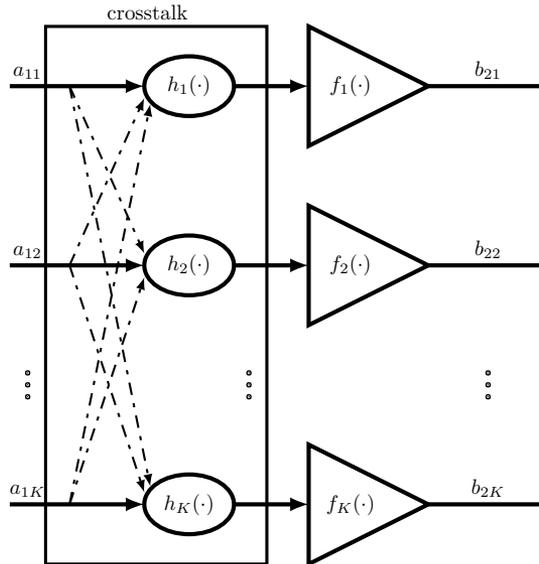
Figure 3.2. System model of a multi-antenna RF transmitter suffering from crosstalk introduced before the PAs.

the signals through a shared local oscillator [38, 39]. The system model of a multi-antenna transmitter suffering from crosstalk introduced before the PAs is shown in Figure 3.2. The output signal of the kth transmit path is given as a linear function $h_k\left(\cdot\right)$ of all PA input signals that describes the crosstalk, followed by a nonlinear function $f_k(\cdot)$ that describes the PA behavior by

$$b_{2k} = f_k\left(h_k\left(a_{11}, \ldots, a_{1K}\right)\right). \tag{3.2}$$

Another system model that is found in literature interprets the output of the kth transmit path as a multi-input nonlinear system

$$b_{2k} = f_k\left(a_{11}, \ldots, a_{1K}\right). \tag{3.3}$$

Note that this system model can be seen as a generalization of the system model in (3.2).

Wideband multi-antenna systems with crosstalk before the PA have been investigated in many papers. The techniques presented in these papers can be divided into two main approaches. Based on the system model in (3.3), the first approach focuses on multivariate nonlinear functions. In [40], the authors propose multivariate polynomial structures including memory effects for the modeling the transmitter output signals. In [41, 42], model and DPD structures for wideband signals are proposed to compensate for crosstalk before the PA. However, the structures proposed in these techniques lack cross-products between signals of different transmit paths that are necessary to fully describe

the nonlinear effects at the PA outputs. Therefore, Abdelhafiz *et al.* [34] extend the proposed structures such that certain cross-products are considered. Amin *et al.* [43] also propose model and predistorter structures based on multivariate polynomials including memory effects to characterize and linearize crosstalk before the PA. Similar structures are used in [44]. Since the complexity of structures based on multivariate polynomials increases rapidly with the number of transmit paths, Zenteno *et al.* [35] propose a sparse estimation technique.

Based on the system model in (3.2), a different approach for the linearization of multi-antenna transmitters has been taken by Suryasarman *et al.* in [31, 45, 46], where a linear crosstalk pre-cancellation scheme is proposed in combination with univariate polynomial-based DPDs. The authors have made use of the knowledge that the crosstalk in the kth path is a linear function of the PA input signals of the other transmitter paths, which is added to the input signal a_{1k}. Hence, an inverse linear function can be applied such that the crosstalk is eliminated from the PA input signal a_{1k} before it even reaches the PA. Conventional single-path DPD can then be used to compensate for the PA nonlinearity. Therefore, the DPD proposed in this work allows for a low complexity implementation [31]. In [47], a further improved version of this technique is proposed.

Note that all techniques presented in literature and mentioned here rely on measurements of all individual transmitter output signals for the identification of the proposed models and predistorters.

Since crosstalk before the PAs has been widely investigated and many solutions, including some with low complexity, have been proposed to model and linearize multi-antenna transmitters suffering from this type of crosstalk, it is not further investigated for the work in this thesis.

3.2.3 Additive Crosstalk After the Power Amplifiers

Mutual coupling between the antennas causes crosstalk and mismatch at the transmitter outputs. Isolators are used to prevent this crosstalk from mixing with the PA output signals. The system model for a multi-antenna transmitter suffering from this type of crosstalk and mismatch shown in Figure 3.3. The output of the kth transmit path is given by

$$b_{2k} = h_k\left(f_1\left(a_{11}\right), \ldots, f_K\left(a_{1K}\right)\right) \tag{3.4}$$

where $f_k(\cdot)$ describes the behavior of the kth PA and $h_k(\cdot)$ describes crosstalk and mismatch as a linear function of all PA output signals. Even though each transmitter output signal is a function of all PA output signals, no nonlinear mixing occurs between the signals from different transmit paths.

Note that, similar to the system model of a transmitter with crosstalk before the PA, the system model of a transmitter with additive mismatch and crosstalk at the PA outputs can also be expressed as a nonlinear function of
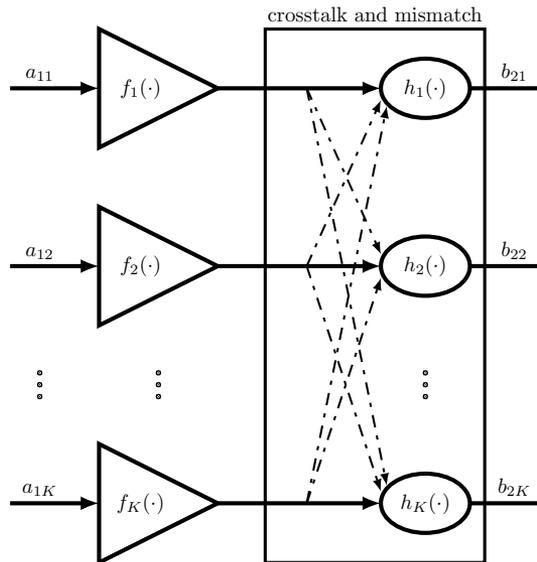
Figure 3.3. System model of a multi-antenna RF transmitter with additive crosstalk and mismatch after the PAs.

the input signals a_{1k} as given in (3.3). However, the system model in (3.2) cannot be applied.

This type of crosstalk is investigated in several papers [34, 40, 41, 42, 43]. For modeling the output of these kinds of systems, a linear combination of several univarite polynomials is suggested. For predistortion, the authors of [34, 40, 43] use similar multivariate polynomial structures as proposed in the same works for the compensation of crosstalk before the PA. In [41, 42], it is suggested to compensate only the PA nonlinear behavior of each path in single-input DPDs at the transmitter. Since this will eliminate all nonlinear distortion, the crosstalk can simply be compensated for at the receiver side of the system, together with channel effects.

Modeling and linearization of transmitters with additive crosstalk after the PAs has been thoroughly investigated and low complexity solutions have been proposed. Therefore, it is not considered necessary to investigate this case further for the work in this thesis.

3.2.4   Antenna Crosstalk and Mismatch

For multi-antenna systems that avoid isolators between the PA outputs and the antennas, antenna crosstalk and mismatch mix with the PA output signals. Hence, this type of antenna crosstalk and mismatch leads to nonlinear effects at the transmitter output. The system model of a multi-antenna RF transmitter suffering from such antenna crosstalk and mismatch is shown in Figure 3.4.
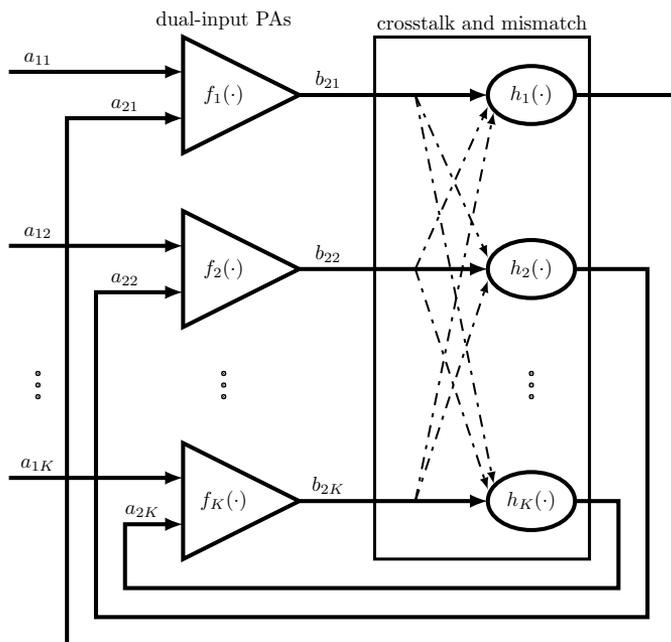
Figure 3.4. System model of a multi-antenna RF transmitter suffering from antenna crosstalk and mismatch.

The system model can be split into two parts [48]. The first part describes the transmitter output signal of the kth path as a nonlinear function of PA input signal, crosstalk and mismatch as

$$b_{2k} = f_k\left(a_{1k}, a_{2k}\right) \tag{3.5}$$

where the signal a_{2k} is the crosstalk and mismatch signal that is incident to the output side of the PA. Here, in contrast to the previously explained system models, $f_k(\cdot)$ is a nonlinear function that describes not only the effects of amplification, but also the effects of crosstalk, including cross-products of the PA output signal with the signal a_{2k}. The PA can therefore be modeled as a dual-input system. The second part of the system model describes the crosstalk and mismatch signal a_{2k} as a function of the transmitter output signals of all transmit paths. Since there are no nonlinear hardware components after the PA, the signal a_{2k} can be described as a linear function of the transmitter output signals by

$$a_{2k} = h_k\left(b_{21}, \ldots, b_{2K}\right). \tag{3.6}$$

This can be interpreted as the system model of the antenna array, since the function $h_k(\cdot)$ depends on the coupling and reflection characteristics of the antenna array.

Note that also this type of transmitter can be modeled as a nonlinear function of the input signals a_{1k} as given in (3.3), but not by the system models in (3.2) and (3.4). It should also be noted that the system model in (3.4) is a special case of the two-part model in (3.5) and (3.6).

From the system model given in (3.5) and (3.6) and shown in Figure 3.4, it is clear that this type of multi-antenna transmitter is more complicated to model and linearize than the previously described cases. The transmitter in this case is a set of dual-input nonlinear functions, the outputs of which are combined through a set of linear systems. The outputs of the linear systems are in turn fed back into the nonlinear systems. Hence, solving the issue of modeling and linearization for wideband systems has not been solved adequately before. However, there are several papers that partially address the problem at hand.

Approaches that are compatible with the system model described by (3.5) and (3.6) have been proposed to model narrowband multi-antenna transmitters suffering from antenna crosstalk. In [7], a dual-input PA model is used in combination with measurements of the antenna array scattering characteristics (S-parameters) to predict the radiation patterns of active antenna arrays. With this technique, the effects of mutual antenna coupling and mismatches on the behavior of PAs and on the performance of a transmit antenna array are investigated. The dual-input PA models in this work are based on polyharmonic distortion (PHD) models [49], and are identified using single-carrier signals. A similar approach is taken in [50]. For their work, the authors use an extended PA model presented in [51] to improve the accuracy. A further extension is proposed in [52]. The PA models in these presented techniques are frequency domain-based and quasi-static. They do not sufficiently take into account dynamic PA distortion. Hence, they are not sufficient for analyzing multi-antenna transmitters driven by wideband signals.

Zargar *et al.* [53] present a dual-input PA model structure that includes memory effects to characterize PAs suffering from source and load mismatch. Cai *et al.* [54] propose and extension to this PA model based on the work presented in [51] and [52]. While these PA model structures are not presented for multi-antenna systems facing antenna crosstalk, they can be applied in this context.

Barradas *et al.* [55] propose a DPD method and identification procedure for the special case of multi-antenna systems with highly correlated input signals, as in phased arrays and beam-steering applications. This method is capable of compensating for PA nonlinearity and dynamic effects as well as the effects of antenna crosstalk and mismatch.

The multivariate polynomial structures proposed in [34, 40, 41, 42, 43] for modeling and linearization of systems with crosstalk before the PA can be applied also for the given problem. This is because the basis functions considered in the proposed structures consider linear and nonlinear combinations of all input signals, which is coincidentally also suitable to describe wideband systems with antenna crosstalk and mismatch. However, these structures are

highly complex and do not scale well for larger numbers of transmit paths.

As can be seen from the literature review, there are open issues in modeling and linearization of multi-antenna systems suffering from antenna crosstalk. Some of these have been investigated for the work presented in this thesis. All the presented work is based on the system model given by (3.5) and (3.6). In Paper A, a modeling technique is presented that combines dual-input PA models based on the memory polynomial structure with linear dynamic antenna array simulations. This technique is suitable to describe the joint effects of PA nonlinearity, antenna crosstalk and mismatch under wideband signal conditions for systems where the crosstalk can be considered relatively small in power. Dedicated model identification procedures are presented as well. An alternative way to identify the dual-input PA models is presented in Paper C. It is shown that the models can be identified from measurements taken by a small number of observations receivers rather than using individual observation receivers to measure every transmit path output. In Paper B, a linearization technique is presented that can compensate for the nonlinear effects due to amplification, antenna crosstalk and mismatch in wideband systems. The technique incorporates knowledge about the system model to reduce complexity for systems with many transmit paths. Details about the proposed solutions and results follow in Chapters 4 and 5.

Chapter 4

Proposed Modeling and Identification Techniques

Since the output of every path of a multi-antenna transmitter depends on more than one input signal, conventional single-input structures are not suitable for modeling such systems. In this chapter, modeling and identification techniques developed during the work on this thesis are presented. First, the modeling technique proposed in Paper A and relevant previously presented approaches are described. Model coefficient identification from input-output measurements of all transmitter output signals, as shown in Paper B, is explained. Alternative identification methods, introduced in Papers A and C, are also described.

4.1 Model Structures

As explained in Chapter 2, it is important that a model structure is capable of describing linear and nonlinear effects, as well as dynamic behavior of the hardware. However, the ideas behind the approaches discussed here can be explained just as well using solely memoryless structures. Hence, in order to avoid cumbersome equations, only equations for memoryless structures are presented here. The equations for structures with memory are given in the appended papers, which are referenced accordingly.

4.1.1 Multi-Input Nonlinear Structures

The output b_{2k} of the kth path of a multi-antenna transmitter can be described as a function of all input signals as given in (3.3). Therefore, multivariate polynomial-based structures can be used to describe b_{2k}. Different versions of such structures are given in [34, 40, 41, 42, 43]. Even though these structures are proposed for transmitters with crosstalk before the PAs, they

can be applied to transmitters with antenna crosstalk and mismatch. E.g., a multivariate memoryless complex polynomial model is given by [40]

$$
b_{2k} = \sum_{i=1}^{K} \theta_{k0i} a_{1i} + \sum_{i_1=1}^{K} \sum_{i_2=i_1}^{K} \sum_{i_3=1}^{K} \theta_{k1i_1 i_2 i_3} a_{1i_1} a_{1i_2} a_{1i_3}^*
$$
$$
+ \sum_{p=2}^{(P-1)/2} \sum_{i_1=1}^{K} \sum_{i_2=i_1}^{K} \cdots \sum_{i_{p+1}=i_p}^{K} \sum_{i_{p+2}=1}^{K} \sum_{i_{p+3}=i_{p+2}}^{K} \cdots
$$
$$
\sum_{i_{2p+1}=i_{2p}}^{K} \theta_{k p i_1 \cdots i_{2p+1}} \prod_{y=1}^{p+1} a_{1i_y} \prod_{z=p+2}^{2p+1} a_{1i_z}^*. \qquad (4.1)
$$

Similar to conventional univariate polynomial structures, multivariate polynomial structures are the sum of different basis functions weighted by complex coefficients and can be expressed by

$$
b_{2k} = \mathbf{G}\left(a_{11}, \ldots, a_{1K}\right) \boldsymbol{\theta}_k. \qquad (4.2)
$$

4.1.2 Dual-Input Nonlinear Structures in Combination with Multi-Input Linear Structures

In Paper A, a different approach is followed. By making direct use of the system model of the transmitter output signals b_{2k} given in (3.5) and the system model of the antenna crosstalk and mismatch signals a_{2k} in (3.6), a combination of two models is proposed: a nonlinear dual-input PA model for each path of the transmitter, and a linear multi-input model of the antenna crosstalk and mismatch characteristics, here referred to as crosstalk and mismatch model (CTMM). The model structures of the two main components of the transmitter can be selected separately.

A suggested CTMM structure describes the antenna crosstalk and mismatch signal of the kth transmit path as a linear combination of all transmitter output signals according to (3.6) as

$$
a_{2k} = \sum_{i=1}^{K} \lambda_{ki} b_{2i} = \boldsymbol{b}_2^T \boldsymbol{\lambda}_k \qquad (4.3)
$$

where $\boldsymbol{b}_2 = [b_{21}, \ldots, b_{2K}]^T$, $\boldsymbol{\lambda}_k = [\lambda_{k1}, \ldots, \lambda_{kK}]^T$, and λ_{ki} are complex coefficients describing the coupling from the ith transmit path to the kth. This model structure is suitable for antenna characteristics that are flat over the signal bandwidth. For frequency dependent antenna behavior, a structure with finite impulse response (FIR) filters can be used, as shown in Paper A.

Bivariate polynomial-based structures fit the description of the dual-input PA system model in (3.5). A memoryless complex polynomial structure is

given by

$$
\begin{aligned}
b_{2k} &= \sum_{p=0}^{(P-1)/2-1} \sum_{v=0}^{p} \sum_{u=0}^{p+1} \theta_{kpvu} \, a_{1k}{}^{p+1-u} a_{1k}^{*}{}^{p-v} a_{2k}{}^{u} a_{2k}^{*}{}^{v} \\
&= \sum_{p=0}^{(P-1)/2} \alpha_{kp} a_{1k}{}^{p+1} a_{1k}^{*}{}^{p} & \text{(4.4a)}
\end{aligned}
$$

$$
+ \sum_{p=0}^{(P-1)/2} \beta_{kp} \, a_{1k}{}^{p} a_{1k}^{*}{}^{p} a_{2k} \tag{4.4b}
$$

$$
+ \sum_{p=1}^{(P-1)/2} \gamma_{kp} \, a_{1k}{}^{p+1} a_{1k}^{*}{}^{p-1} a_{2k}^{*} \tag{4.4c}
$$

$$
+ \sum_{p=1}^{(P-1)/2} \sum_{v=0}^{p} \sum_{\substack{u=0 \\ u>1-v}}^{p+1} \delta_{kpuv} a_{1k}{}^{p+1-u} a_{1k}^{*}{}^{p-v} a_{2k}{}^{u} a_{2k}^{*}{}^{v} \tag{4.4d}
$$

where $\alpha_{kp}, \beta_{kp}, \gamma_{kp}, \delta_{kpuv}$ are complex-valued coefficients. The structure has four types of basis functions: basis functions that depend only on a_{1k} in (4.4a), which describe the behavior of the PA due to the amplification of a_{1k}. These basis functions are the same as in the single-input polynomial model in (2.5). Basis functions that depend on a_{1k} and linear terms of a_{2k} are given in (4.4b), basis functions that depend on a_{1k} and linear terms of a_{2k}^{*} in (4.4c), and basis functions that depend on a_{1k} and nonlinear terms of a_{2k} in (4.4d). The last three types of basis functions describe the effects of coupling and mismatch, and the mixing of these effects with PA nonlinearity. If the crosstalk and mismatch signal a_{2k} can be considered relatively small in power, only linear terms of a_{2k} need to be considered in the dual-input PA models [53]. Then, all basis functions in (4.4d) become negligible and can be set to zero. Extended complex polynomial structures including memory are given in Papers A and B. In the convenient notation using basis functions, (4.4) is written as

$$
b_{2k} = \begin{bmatrix} \mathbf{G}^{(0)}(a_{1k}) & \mathbf{G}^{(1)}(a_{1k}, a_{2k}) & \mathbf{G}^{(2)}(a_{1k}, a_{2k}) & \mathbf{G}^{(3)}(a_{1k}, a_{2k}) \end{bmatrix} \begin{bmatrix} \boldsymbol{\alpha}_{k} \\ \boldsymbol{\beta}_{k} \\ \boldsymbol{\gamma}_{k} \\ \boldsymbol{\delta}_{k} \end{bmatrix}
$$

$$
= \mathbf{G}(a_{1k}, a_{2k}) \boldsymbol{\theta}_{k}. \tag{4.5}
$$

It is shown in Paper A that after inserting the expression given in (4.3) in (4.4), a time-stepped solution can be found for all b_{2k}. Once all model coefficients have been identified, this solution can be used to predict the output signals of the transmitter for a specific set of input signals. The time-stepped method for prediction of the transmitter outputs is given in Algorithm 4.1. Different methods for identification of the model coefficients are presented in Section 4.2.

The derivations for models including memory effects are considerably more involved. These are shown in Paper A. Note that only systems with relatively small power levels of crosstalk and mismatch are investigated in Paper A, where model structures with only linear terms of a_{2k} are considered.

The proposed approach can be directly compared to the approaches in [7, 50, 52]. The difference between these approaches and the work presented in Paper A is that the structures in Paper A are derived in time domain and include memory effects, which makes them suitable for wideband signal conditions.

Algorithm 4.1 Prediction of transmitter output signals using the proposed modeling approach.

Inputs: input signals a_{1k}

Known from identification: PA model coefficients α_{kp}, β_{kp}, γ_{kp}

$\qquad\qquad\qquad\qquad$ CTMM coefficients $\boldsymbol{\Lambda} = [\boldsymbol{\lambda}_1, \ldots, \boldsymbol{\lambda}_K]^T$

for all time samples n **do**

$\qquad$ **for all** k **do**

$\qquad\qquad f_k^{(0)} = \sum_{p=0}^{(P-1)/2} \alpha_{kp} a_{1k}{}^{p+1} a_{1k}^{*}{}^{p}$

$\qquad\qquad f_k^{(1)} = \sum_{p=0}^{(P-1)/2} \beta_{kp} a_{1k}{}^{p} a_{1k}^{*}{}^{p}$

$\qquad\qquad f_k^{(2)} = \sum_{p=1}^{(P-1)/2} \gamma_{kp} a_{1k}{}^{p+1} a_{1k}^{*}{}^{p-1}$

$\qquad$ **end for**

$\qquad \mathbf{f}^{(0)} = \left[f_1^{(0)}, \ldots, f_K^{(0)} \right]^T$

$\qquad \mathbf{F}^{(1)} = \mathrm{diag}\left\{ f_1^{(1)}, \ldots, f_K^{(1)} \right\}$

$\qquad \mathbf{F}^{(2)} = \mathrm{diag}\left\{ f_1^{(2)}, \ldots, f_K^{(2)} \right\}$

$\qquad \begin{bmatrix} \Re\{\boldsymbol{b}_2\} \\ \Im\{\boldsymbol{b}_2\} \end{bmatrix} = \begin{bmatrix} \mathbf{I} + \Re\left\{ -\mathbf{F}^{(1)}\boldsymbol{\Lambda} - \mathbf{F}^{(2)}\boldsymbol{\Lambda}^* \right\} & \Im\left\{ \mathbf{F}^{(1)}\boldsymbol{\Lambda} - \mathbf{F}^{(2)}\boldsymbol{\Lambda}^* \right\} \\ \Im\left\{ -\mathbf{F}^{(1)}\boldsymbol{\Lambda} - \mathbf{F}^{(2)}\boldsymbol{\Lambda}^* \right\} & \mathbf{I} + \Re\left\{ -\mathbf{F}^{(1)}\boldsymbol{\Lambda} + \mathbf{F}^{(2)}\boldsymbol{\Lambda}^* \right\} \end{bmatrix}^{+}$

$\qquad\qquad \times \begin{bmatrix} \Re\left\{ \mathbf{f}^{(0)} \right\} \\ \Im\left\{ \mathbf{f}^{(0)} \right\} \end{bmatrix}$ where $\boldsymbol{b}_2 = [b_{21}, \ldots, b_{2k}]^T$

$\qquad \boldsymbol{b}_2 = \Re\{\boldsymbol{b}_2\} + j\Im\{\boldsymbol{b}_2\}$

end for

Outputs: predicted output signals b_{2k} for all n, k

4.2 Model Coefficient Identification

The identification of model coefficients is usually done from measurements of the individual transmitter output signals for known input signals. When using multi-input model structures, this is straightforward. However, for the

model structures presented in Section 4.1.2, the identification procedure is not so trivial. An identification procedure using measurements of the transmitter output signals is proposed in Paper B. Another procedure, where measurements of the individual transmitter components are performed, is proposed in Paper A. A third alternative using over-the-air measurements of a small number of observation receivers is presented in Paper C.

4.2.1 From Measurements of Transmitter Output Signals

The coefficients of models based on multi-input structures can be identified using linear least-squares techniques. Based on a measurement of the kth transmitter output signal $\mathbf{b}_{2k}$, the model coefficients for the kth path of the transmitter are found by

$$\boldsymbol{\theta}_{k,LS} = \mathbf{G}\left(\mathbf{a}_{11}, \ldots, \mathbf{a}_{1K}\right)^+ \mathbf{b}_{2k}. \tag{4.6}$$

For the technique proposed in Paper A and described in Section 4.1.2, the model coefficient identification has to include both the dual-input PA model coefficients and the coefficients of the CTMM. In Paper B, a two-step identification procedure is presented to identify all these coefficients. In step 1, using an estimate of the CTMM coefficients, the PA model coefficients are estimated. In step 2, using the estimated PA coefficients, the CTMM coefficients are estimated. Both steps are performed in several iterations until a satisfying result is reached. The procedure is described in Algorithm 4.2. Note that the solution for CTMM coefficients and dual-input PA coefficients is not unique. A procedure is suggested in Paper B to avoid problems arising from this.

For the model identification from transmitter output measurements, the input signals to the transmitter must not be fully correlated.

Experimental Results

The reliability of the extraction method explained in Algorithm 4.2 was evaluated using measurement of a four-path transmitter. Four identical GaAs PA evaluation boards from Skyworks (SKY66001-11) [56] were used, which were supplied with 3.3 V and operated at a center frequency of 2.12 GHz. The antenna array was a rectangular four-element array with microstrip patch elements. The highest coupling factor between two elements of the array was around -12 dB. Couplers were used at the PA outputs to measure the individual transmitter output signals. The bandwidth of the input signals was 5 MHz, and the sampling rate of the system was 25 MHz.

In order to investigate the reliability of the proposed extraction method, CTMM coefficients and dual-input PA model coefficients were identified for different initial values $\tilde{\boldsymbol{\lambda}}_k^{(0)}$. The results were compared to confirm convergence. The initial values were complex numbers with real and imaginary parts that were randomly chosen according to a uniform distribution with interval $[1, 1]$. The procedure recommended in Paper B to avoid numerical and

Algorithm 4.2 Procedure for the joint identification of dual-input PA model coefficients and CTMM coefficients of the kth transmit path from measurements of the transmitter output signals.

Inputs: input signals $\mathbf{a}_{1k}$

Known from measurements: all output signals $\mathbf{b}_{2k}$, $\mathbf{B}_2 = [\mathbf{b}_{21}, \ldots, \mathbf{b}_{2K}]$

INITIAL STEP $i = 0$

$\text{NMSE}_{des} = X$ $\triangleright$ define desired accuracy

$\tilde{\boldsymbol{\lambda}}_k^{(0)} = \mathbf{1}$ $\triangleright$ set initial value of CTMM coefficients

$\tilde{\mathbf{a}}_{2k}^{(0)} = \mathbf{B}_2 \tilde{\boldsymbol{\lambda}}_k^{(0)}$

$\text{NMSE} = \infty$

while $\text{NMSE} \geq \text{NMSE}_{des}$ **do** $\triangleright$ iterate until desired accuracy is reached

     $i = i + 1$

     STEP 1: find PA model coefficients

     $\tilde{\boldsymbol{\theta}}_k^{(i)} = \mathbf{G}\left(\mathbf{a}_{1k}, \tilde{\mathbf{a}}_{2k}^{(i-1)}\right)^+ \mathbf{b}_{2k}$

     STEP 2: find CTMM coefficients

     for all time samples n **do**

         $f_k^{(0)} = \sum_{p=0}^{(P-1)/2} \tilde{\alpha}_{kp}\, a_{1k}{}^{p+1} a_{1k}^*{}^{p}$

         $f_k^{(1)} = \sum_{p=0}^{(P-1)/2} \tilde{\beta}_{kp}\, a_{1k}{}^{p} a_{1k}^*{}^{p}$

         $f_k^{(2)} = \sum_{p=1}^{(P-1)/2} \tilde{\gamma}_{kp}\, a_{1k}{}^{p+1} a_{1k}^*{}^{p-1}$

         $f_k^{(3)} = \sum_{p=1}^{(P-1)/2}\sum_{v=0}^{p}\sum_{\substack{u=0 \\ u>1-v}}^{p+1} \tilde{\delta}_{kpuv}\, a_{1k}{}^{p+1-u} a_{1k}^*{}^{p-v}\left(\tilde{a}_{2k}^{(i-1)}\right)^u \left(\tilde{a}_{2k}^{*(i-1)}\right)^v$

     end for

     $\mathbf{F}_k^{(1)} = \text{diag}\left\{\mathbf{f}_k^{(1)}\right\} \mathbf{B}_2$ $\mathbf{F}_k^{(2)} = \text{diag}\left\{\mathbf{f}_k^{(2)}\right\} \mathbf{B}_2^*$

     $\begin{bmatrix} \Re\left\{\tilde{\boldsymbol{\lambda}}_k^{(i)}\right\} \\ \Im\left\{\tilde{\boldsymbol{\lambda}}_k^{(i)}\right\} \end{bmatrix} = \begin{bmatrix} \Re\left\{\mathbf{F}_k^{(1)}+\mathbf{F}_k^{(2)}\right\} & \Im\left\{-\mathbf{F}_k^{(1)}+\mathbf{F}_k^{(2)}\right\} \\ \Im\left\{\mathbf{F}_k^{(1)}+\mathbf{F}_k^{(2)}\right\} & \Re\left\{\mathbf{F}_k^{(1)}-\mathbf{F}_k^{(2)}\right\} \end{bmatrix}^+ \begin{bmatrix} \Re\left\{\mathbf{b}_{2k}-\mathbf{f}_k^{(0)}-\hat{\mathbf{f}}_k^{(3)}\right\} \\ \Im\left\{\mathbf{b}_{2k}-\mathbf{f}_k^{(0)}-\hat{\mathbf{f}}_k^{(3)}\right\} \end{bmatrix}$

     $\tilde{\boldsymbol{\lambda}}_k^{(i)} = \Re\left\{\tilde{\boldsymbol{\lambda}}_k^{(i)}\right\} + j\Im\left\{\tilde{\boldsymbol{\lambda}}_k^{(i)}\right\}$

     $\tilde{\boldsymbol{\lambda}}_k^{(i)} := \tilde{\boldsymbol{\lambda}}_k^{(i)} / \max_{j=1,\ldots,K;j\neq k}\left\{\tilde{\lambda}_{kj}^{(i)}\right\}$ $\tilde{\lambda}_{kk}^{(i)} = 1$ $\triangleright$ normalization

     $\tilde{\mathbf{a}}_{2k}^{(i)} = \mathbf{B}_2 \tilde{\boldsymbol{\lambda}}_k^{(i)}$

     $\tilde{\mathbf{b}}_{2k}^{(i)} = \mathbf{G}\left(\mathbf{a}_{1k}, \tilde{\mathbf{a}}_{2k}^{(i)}\right) \tilde{\boldsymbol{\theta}}_k^{(i)}$

     $\text{NMSE} = \text{NMSE}\left(\mathbf{b}_{2k}, \tilde{\mathbf{b}}_{2k}^{(i)}\right)$

end while

Outputs: CTMM coefficients for kth transmit path $\boldsymbol{\lambda}_{k,ID} = \tilde{\boldsymbol{\lambda}}_k^{(i)}$

               PA model coefficients for kth transmit path $\boldsymbol{\theta}_{k,ID} = \tilde{\boldsymbol{\theta}}_k^{(i)}$
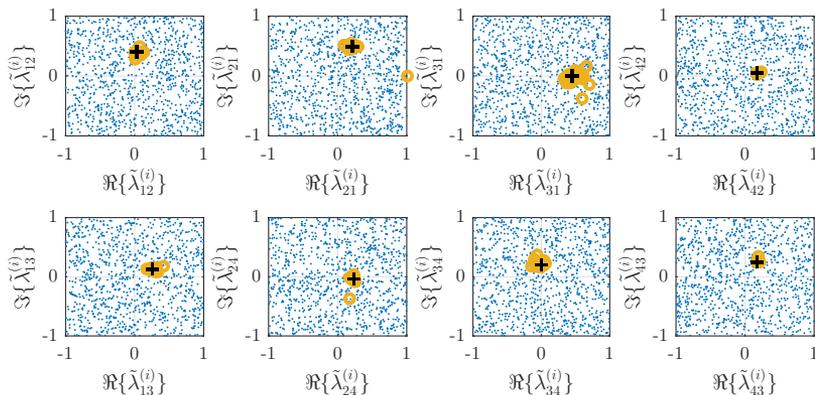

Figure 4.1. Reliability of the technique proposed for model extraction from measurements of the transmitter output signals: identified CTMM coefficients for different initial values. Initial values are shown as blue dots, the results after the first iteration as yellow circles, and the results after the second iteration as black plus signs. The results converge such that no difference can be noticed after the second iteration. Since the kth CTMM coefficient and the maximum CTMM coefficient of the kth transmit path assume the fixed value 1, only the results for the remaining eight CTMM coefficients are shown.

identification problems was used, where the kth CTMM coefficient and the maximum CTMM coefficient of the kth transmit path assume the fixed value 1. Figure 4.1 shows results for identification of the remaining CTMM coefficients. Each blue dot represents an initial value. The yellow circles show the results after the first iteration, and the black plus signs show the results after the second iteration. The results converge to the same value for all initial values. After two iterations, no difference between the results for different initial values can be noticed. The NMSEs between the measured transmitter output signals and the modeled transmitter output signals were -39.3 dB for path 1, -38.6 dB for path 2, -38.6 dB for path 3 and -38.9 dB for path 4.

4.2.2   From Measurements of Individual Hardware Components

In Paper B, it is shown that the dual-input PA model coefficients and the CTMM coefficients can be identified from measurements of the individual hardware components or from circuit/antenna simulation. The suggested identification procedure is very useful for evaluating the performance of multi-antenna transmitters in an early design stage. Since it is not necessary to implement the complete transmitter in order to extract model coefficients, it is possible to evaluate and compare system performance for different types of hardware components without great effort. Coefficients for multi-input structures cannot be found this way.
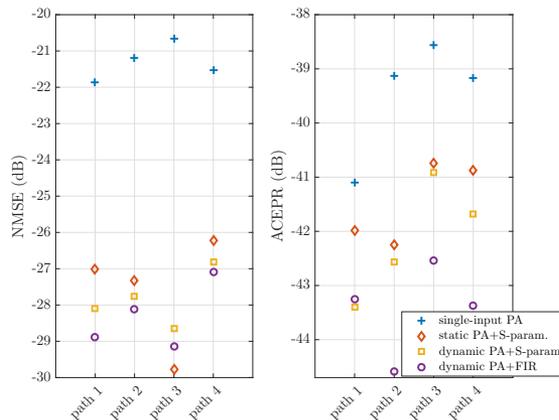
Figure 4.2. Evaluation of the proposed modeling technique when using model extraction from measurements of individual hardware components: NMSE (left) and ACEPR (right) between measured and simulated transmitter output. Results are shown for: single-input PA model structures that do not consider antenna crosstalk (blue +), the proposed technique with quasi-static PA model structures and single-frequency S-parameter CTMM (red ◊), the proposed technique with memory polynomial PA model structures and single-frequency S-parameter CTMM (yellow □), the proposed technique with memory polynomial PA model structures and FIR filter-based CTMM (purple ○).

The CTMM coefficients in (4.3) are the single-frequency S-parameters at the center frequency of the system. These can be obtained from measurements with a vector network analyzer (VNA) or from simulations. For an FIR filter description of the antenna array characteristics, the model coefficients can be found from measurements or simulations of the S-parameters over a range of frequencies.

The dual-input PA model coefficients in (4.5) are identified using active loadpull measurements [57], [58]. In such measurements, different signals are injected at the input and output side of a PA. The PA input and output signals, i.e., a_{1k}, b_{1k}, a_{2k}, and b_{2k}, are synchronously measured at calibrated reference planes. The model coefficients are found by

$$\boldsymbol{\theta}_{k,LS} = \mathbf{G}\left(\mathbf{a}_{1k}, \mathbf{a}_{2k}\right)^{+} \mathbf{b}_{2k}. \qquad (4.7)$$

Experimental Results

The proposed technique and model extraction method were validated using measurements of a four-path transmitter. The same transmitter as described in Section 4.2.1 was used. The bandwidth of the input signals was 20 MHz, and the sampling rate of the system was 100 MHz.

First, all model coefficients were extracted from measurements of the individual transmitter components. Then, the transmitter was implemented in
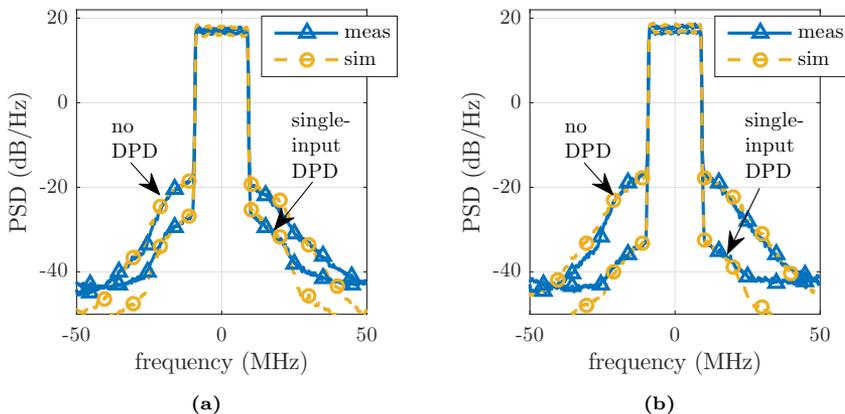
Figure 4.3. Evaluation of the proposed modeling technique when using model extraction from measurements of individual hardware components: Spectra of the transmitter output of path 1 for (a) high-coupling array and (b) low-coupling array. Measurements (meas) without DPD and with single-input DPD are compared to simulations (sim) without DPD and with single-input DPD.

the lab. Measurements of the transmitter output signals were compared to the predicted output signals given by a simulation using the extracted models. The results for the following model structures are evaluated in Figure 4.2: single-input PA model structures that do not consider antenna crosstalk, the proposed technique with quasi-static PA model structures and single-frequency S-parameter CTMM, the proposed technique with memory polynomial PA model structures and single-frequency S-parameter CTMM, the proposed technique with memory polynomial PA model structures and FIR filter-based CTMM. Clearly, using single-input PA models that ignore crosstalk and mismatch gives the worst performance. Overall, the best performance is reached by the proposed technique with dynamic PA models in combination with an FIR CTMM, followed by the dynamic PA models in combination with a single-frequency S-parameter CTMM, and the quasi-static PA models combined with a single-frequency S-parameter CTMM.

An example of how the proposed method can be used to analyze the performance of a multi-antenna transmitter is also given. In this example, it was investigated how well simple single-input predistortion can eliminate the effects of PA nonlinearity and crosstalk. Simulations and measurements were performed for two different antenna arrays: the array with maximum coupling of -12 dB, and an array with maximum coupling of -24 dB. Single-input DPD was applied in all transmitter paths. The power spectral densities (PSDs) of the transmitter output of path 1 are shown in Figure 4.3. In Figure 4.3a, the results for the array with higher coupling are given, and in Figure 4.3b, the results for the array with lower coupling are given. As can be seen, the

simulation with the proposed method predicts the measured results well. The presented results demonstrate the usefulness of the proposed method for investigating different system components and for algorithm testing. In this example, it is clear that single-input DPD cannot compensate for all nonlinear distortion and that more advanced DPD algorithms need to be used. It can also be seen that less nonlinear distortion is present when using the array with the lower coupling.

A more detailed validation of the proposed method is presented in Paper B. Application examples can be found in [59, 60].

4.2.3   From Over-the-Air Measurements

Hardware cost and complexity are a big concern in multi-antenna systems. Using an observation receiver with a full receiver chain at each transmitter becomes infeasible for transmitters with large numbers of paths. However, for predistortion purposes it is often necessary to monitor the behavior of the system while operating, since the characteristics can change over time, for example due to temperature changes and aging of the components. One way of reducing hardware complexity is using time-shared observation receivers [47, 61]. For such a solution, couplers after the PA outputs feed the transmitter output signals to a receiver path where a switch alternately selects between the different transmit paths, such that one transmitter output is measured at a time. This solution can suffer from interference between the different transmit signals due to imperfect isolation in the selector switch [62]. Therefore, an identification technique is presented in Paper C, where the transmitter output signals are measured over the air, i.e., a small number of observation receivers is utilized to measure transmissions from several or all branches at the same time. These receivers could be connected to dedicated listening antennas within the transmit array, or placed in the far field of the transmitter. The proposed technique is developed for the identification of the dual-input PA coefficients in (4.5), while the the CTMM coefficients in (4.3) are assumed to be known. The CTMM coefficients can be found from simulations or measurements of the antenna array S-parameters, as explained in Section 4.2.2.

A block diagram of a multi-antenna transmitter with K transmit paths and L over-the-air observation receivers is shown in Figure 4.4. Each of the K transmit branches is coupled to each of the L observation receivers with the channel coefficients η_{lk}, $k = 1, \ldots, K$ and $l = 1, \ldots, L$. The channel coefficients are assumed to be known. If the receiver antennas are placed within the same array as the transmitter antennas, S-parameter measurements or simulations can be performed to identify the channel coefficients. If the receiver antennas are placed in a separate receiver array, or individual receiver antennas in completely separate locations in the far-field of the transmitter are used, channel estimation is required. The received signal at the lth receiver is
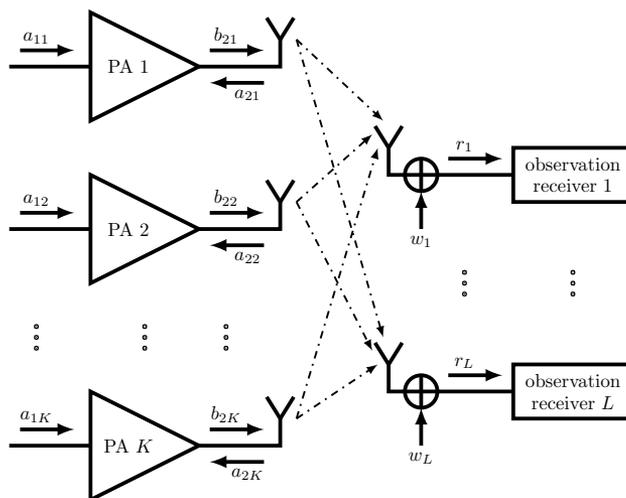
Figure 4.4. Block diagram of a multi-antenna transmitter with K transmit paths and L over-the-air observation receivers.

given as a linear combination of all K transmitter outputs by

$$r_l = \sum_{k=1}^{K} \eta_{lk} b_{2k} + w_l = \sum_{k=1}^{K} \eta_{lk} \mathbf{G} \left(a_{1k}, a_{2k} \right) \boldsymbol{\theta}_k + w_l \tag{4.8}$$

where w_l is complex additive white Gaussian noise (AWGN) added at the lth receiver input. This is extended to a matrix equation describing all received signals as

$$\begin{bmatrix} \mathbf{r}_1 \\ \vdots \\ \mathbf{r}_L \end{bmatrix} = \begin{bmatrix} \eta_{11} \mathbf{G} \left(\mathbf{a}_{11}, \mathbf{a}_{21} \right) & \cdots & \eta_{1K} \mathbf{G} \left(\mathbf{a}_{1K}, \mathbf{a}_{2K} \right) \\ \vdots & \ddots & \vdots \\ \eta_{L1} \mathbf{G} \left(\mathbf{a}_{11}, \mathbf{a}_{21} \right) & \cdots & \eta_{LK} \mathbf{G} \left(\mathbf{a}_{1K}, \mathbf{a}_{2K} \right) \end{bmatrix} \begin{bmatrix} \boldsymbol{\theta}_1 \\ \vdots \\ \boldsymbol{\theta}_K \end{bmatrix} + \begin{bmatrix} \mathbf{w}_1 \\ \vdots \\ \mathbf{w}_L \end{bmatrix}$$

$$\mathbf{r} = \begin{bmatrix} \boldsymbol{\eta}_1 \otimes \mathbf{G} \left(\mathbf{a}_{11}, \mathbf{a}_{21} \right) & \cdots & \boldsymbol{\eta}_K \otimes \mathbf{G} \left(\mathbf{a}_{1K}, \mathbf{a}_{2K} \right) \end{bmatrix} \boldsymbol{\theta} + \mathbf{w} \tag{4.9}$$

where $\boldsymbol{\eta}_k = [\eta_{1k}, \ldots, \eta_{Lk}]^T$. Furthermore, $\mathbf{r}$ includes the received signal vectors $\mathbf{r}_l$ of all receivers, $\mathbf{w}$ includes all noise vectors $\mathbf{w}_l$, $\boldsymbol{\theta}$ contains all PA model coefficient vectors $\boldsymbol{\theta}_k$ and $\otimes$ denotes the Kronecker product.

In Paper C it is shown that PA model coefficients can be identified using an iterative procedure. Measurements with at least two observation receivers are required for this procedure. The identification procedure is explained in Algorithm 4.3.

Note that for a multi-antenna transmitter without crosstalk, the measurement of only one single observation receiver can be sufficient to identify all PA model coefficients using simple least-squares estimation for the identification [62, 63]. The signal received by the single observation receiver in such a

transmitter is given by

$$\mathbf{r}_1 = \begin{bmatrix} \eta_{11}\mathbf{G}\left(\mathbf{a}_{11}\right) & \cdots & \eta_{1K}\mathbf{G}\left(\mathbf{a}_{1K}\right) \end{bmatrix} \boldsymbol{\theta} + \mathbf{w}_1 \qquad (4.10)$$

such that the least-squares solution $\boldsymbol{\theta}_{LS}$ of the all PA model coefficients is obtained by

$$\boldsymbol{\theta}_{LS} = \begin{bmatrix} \eta_{11}\mathbf{G}\left(\mathbf{a}_{11}\right) & \cdots & \eta_{1K}\mathbf{G}\left(\mathbf{a}_{1K}\right) \end{bmatrix}^{+} \mathbf{r_1}. \qquad (4.11)$$

For the PA model identification from over-the-air measurements, the input signals to the transmitter must not be fully correlated.

Algorithm 4.3 Procedure for the identification of dual-input PA model coefficients $\boldsymbol{\theta}_k$ from over-the-air measurements with at least two observation receivers, where the CTMM coefficients $\boldsymbol{\lambda}_k$ and channel coefficients $\boldsymbol{\eta}_k$ are known.

Inputs: input signals $\mathbf{a}_{1k}$

         CTMM coefficients $\boldsymbol{\lambda}_k = [\lambda_{k1}, \ldots, \lambda_{kK}]^T$

         channel coefficients $\boldsymbol{\eta}_k = [\eta_{1k}, \ldots, \eta_{Lk}]^T$

Known from measurements: received signals $\mathbf{r} = [\mathbf{r}_1^T, \ldots, \mathbf{r}_L^T]^T$, $L \geq 2$

INITIAL STEP $i = 0$

$\mathrm{NMSE}_{des} = X$ $\triangleright$ define desired accuracy

$\tilde{\mathbf{B}}_2^{(0)} = \left[\tilde{\mathbf{b}}_{21}^{(0)}, \ldots, \tilde{\mathbf{b}}_{2K}^{(0)}\right] = \mathbf{0}$ $\triangleright$ set initial values of PA model outputs

$\mathrm{NMSE} = \infty$

while $\mathrm{NMSE} \geq \mathrm{NMSE}_{des}$ **do** $\triangleright$ iterate until desired accuracy is reached

     $i = i + 1$

     compute for all k: $\tilde{\mathbf{a}}_{2k}^{(i)} = \tilde{\mathbf{B}}_2^{(i-1)}\boldsymbol{\lambda}_k$

     $\tilde{\boldsymbol{\theta}}^{(i)} = \begin{bmatrix} \boldsymbol{\eta}_1 \otimes \mathbf{G}\left(\mathbf{a}_{11}, \tilde{\mathbf{a}}_{21}^{(i)}\right) & \cdots & \boldsymbol{\eta}_K \otimes \mathbf{G}\left(\mathbf{a}_{1K}, \tilde{\mathbf{a}}_{2K}^{(i)}\right) \end{bmatrix}^{+} \mathbf{r}$

                                               $\triangleright$ $\tilde{\boldsymbol{\theta}} = [\tilde{\boldsymbol{\theta}}_1^T, \ldots, \tilde{\boldsymbol{\theta}}_K^T]^T$

     $\tilde{\mathbf{B}}_2^{(i)} = \begin{bmatrix} \mathbf{G}\left(\mathbf{a}_{11}, \tilde{\mathbf{a}}_{21}^{(i)}\right)\tilde{\boldsymbol{\theta}}_1^{(i)} & \cdots & \mathbf{G}\left(\mathbf{a}_{1K}, \tilde{\mathbf{a}}_{2K}^{(i)}\right)\tilde{\boldsymbol{\theta}}_K^{(i)} \end{bmatrix}$

     $\begin{bmatrix} \tilde{\mathbf{r}}_1^{(i)} & \cdots & \tilde{\mathbf{r}}_L^{(i)} \end{bmatrix} = \tilde{\mathbf{B}}_2^{(i)} \begin{bmatrix} \boldsymbol{\eta}_1 & \cdots & \boldsymbol{\eta}_K \end{bmatrix}^T$

     $\mathrm{NMSE} = \max\limits_{l=1,\ldots,L} \left\{ \mathrm{NMSE}\left(\mathbf{r}_l, \tilde{\mathbf{r}}_l^{(i)}\right) \right\}$

end while

Outputs: PA model coefficients $\boldsymbol{\theta}_{k,ID} = \tilde{\boldsymbol{\theta}}_k^{(i)}$ for all K transmit paths

---

Simulation Results

The proposed model identification method was evaluated in simulations of a multi-antenna transmitter. The simulator was implemented as described

in Algorithm 4.1. For the simulator PAs, coefficients of sixty-two different dual-input PA models were extracted from measurements obtained from the transmitter setup explained in Section 4.2.1. Even though extracted from only four different PAs, the models exhibit stochastic variations since they were extracted from different measurement sets. Each model was based on complex polynomials with highest polynomial order $P = 5$. A rectangular 8×8 antenna array was used, were the highest coupling between two elements was -12 dB. The observation receivers were connected to dedicated antennas within the transmit array. The array S-parameters, i.e., the CTMM and channel coefficients, were obtained in simulations. The input signals were independent OFDM signals with 5 MHz bandwidth, and the baseband sampling frequency was 25 MHz.

The proposed model identification was tested for different simulator settings. Figure 4.5 shows the NMSEs between the simulated transmitter output signals and the modeled output signals for every individual transmit path for signal-to-noise ratios (SNRs) of 60 dB and 40 dB with $N = 12500$ samples, two observation receivers and sixty-two transmit paths. The results for high SNR are very good, with a maximum NMSE of -43 dB. The results for low SNR are not satisfying. To obtain better model results for a given SNR, the number of observation receivers or the number of samples can be increased. Figure 4.6 shows modeling results for 40 dB SNR with (a) four receivers and $N = 12500$, and (b) two receivers and $N = 375000$. The results show that it is possible to identify PA model coefficients using the proposed over-the-air identification method. Good results can be obtained even for low receiver SNRs if the number of receivers and the number of samples are well chosen.
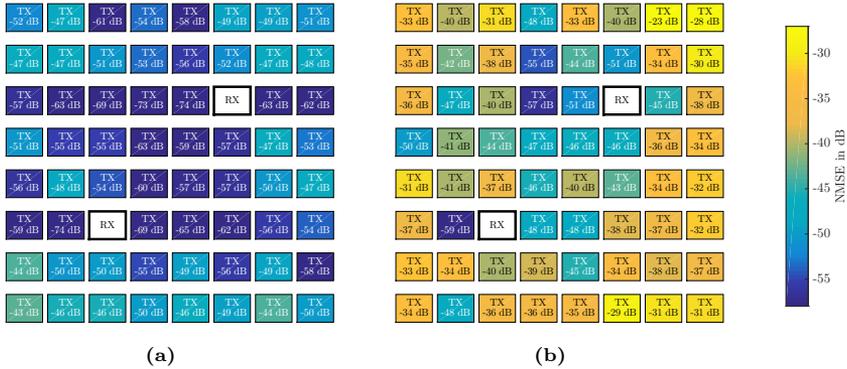
Figure 4.5. Evaluation of the technique proposed for PA model extraction from over-the-air measurements for an 8×8 array with two observation receivers and sixty-two transmit paths: NMSEs in dB of the transmitter output signals for each individual transmit path for $N = 12500$ and (a) 60 dB SNR, (b) 40 dB SNR. The position of receiver antennas is indicated by RX, and the position of transmitter antennas is indicated by TX.

Figure 4.6. Evaluation of the technique proposed for PA model extraction from over-the-air measurements for an 8×8 array: NMSEs in dB for each individual transmit path for 40 dB SNR with (a) four observation receivers, sixty transmit paths and $N = 12500$; (b) two observation receivers, sixty-two transmit paths and $N = 375000$. The position of receiver antennas is indicated by RX, and the position of transmitter antennas is indicated by TX.

Chapter 5

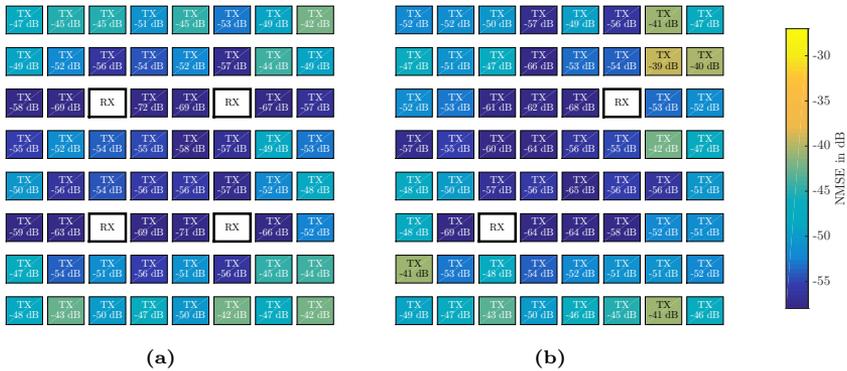# Proposed Digital Predistortion Technique

Linearization techniques for multi-antenna RF transmitters need to compensate for the joint effects of PA nonlinearity, antenna crosstalk and mismatch. In order to make a predistorter structure suitable for implementation in dedicated hardware, it is important that the complexity is kept low. In this chapter, the DPD techniques designed during the work for this thesis are presented. First, the DPD method proposed in Paper B is described and compared to other approaches. Then, a technique to identify DPD from over-the-air measurements, as proposed in Paper C, is explained.

5.1 Predistorter Structures

As for conventional single-input systems, DPD structures for multi-antenna systems can be based on structures that are also suitable for modeling the same system.

5.1.1 Multi-Input DPD

A possible predistorter structure is the multi-input PA model structure given in (4.1). Examples including memory effects can be found in [40, 41, 42, 34, 43], where the structures are used to compensate for crosstalk before the PA. A predistorter with such a structure has to be used in every transmit path. The block diagram of a multi-antenna transmitter with a multi-input predistorter in every transmit path is shown in Figure 5.1. For such structures, the predistorted signal for the kth transmit path is given as a function of the desired transmit signals of all paths by

$$a_{1k} = \hat{\mathbf{G}} \left(b_{d1}, \ldots, b_{dK} \right) \hat{\boldsymbol{\theta}}_k \tag{5.1}$$
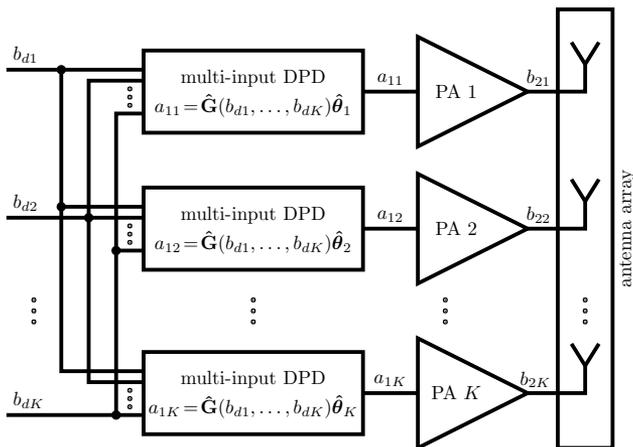
Figure 5.1. Block diagram of a multi-antenna transmitter with multi-input DPDs.

where $\hat{\boldsymbol{\theta}}_k$ are the predistorter coefficients of the kth multi-input predistorter. Basis functions need to include all possible combinations and cross-terms for all signals. Hence, the number of predistorter coefficients and thus the complexity of such structures does not scale well with the number of transmit paths.

5.1.2 Dual-Input DPD in Combination with a Crosstalk and Mismatch Model

In Paper B, a predistorter structure that is based on the the transmitter model in Paper A is proposed. The proposed DPD consists of two main blocks: one linear crosstalk and mismatch model (CTMM) block shared by all transmit paths, and a dual-input DPD block in every transmit path. A block diagram of the proposed method is shown in Figure 5.2. Each dual-input DPD block is the inverse function of the respective dual-input PA. The CTMM block emulates the behavior of the antenna array.

The CTMM block produces the signals $\tilde{a}_{2k}$, which are an estimate of the crosstalk and mismatch signals a_{2k}, by

$$\tilde{a}_{2k} = \boldsymbol{b}_d^T \boldsymbol{\lambda}_k. \tag{5.2}$$

where $\boldsymbol{b}_d = [b_{d1}, \ldots, b_{dK}]^T$ is a vector with the desired signals of all transmit paths, and $\boldsymbol{\lambda}_k$ are the CTMM coefficients.

The predistorted signal for the kth transmit path is given as a function of the desired signal of the kth path and the estimated crosstalk signal $\tilde{a}_{2k}$ by

$$a_{1k} = \hat{\mathbf{G}} \left(b_{dk}, \tilde{a}_{2k} \right) \hat{\boldsymbol{\theta}}_k \tag{5.3}$$

where $\hat{\boldsymbol{\theta}}_k$ are the predistorter coefficients of the kth dual-input predistorter.
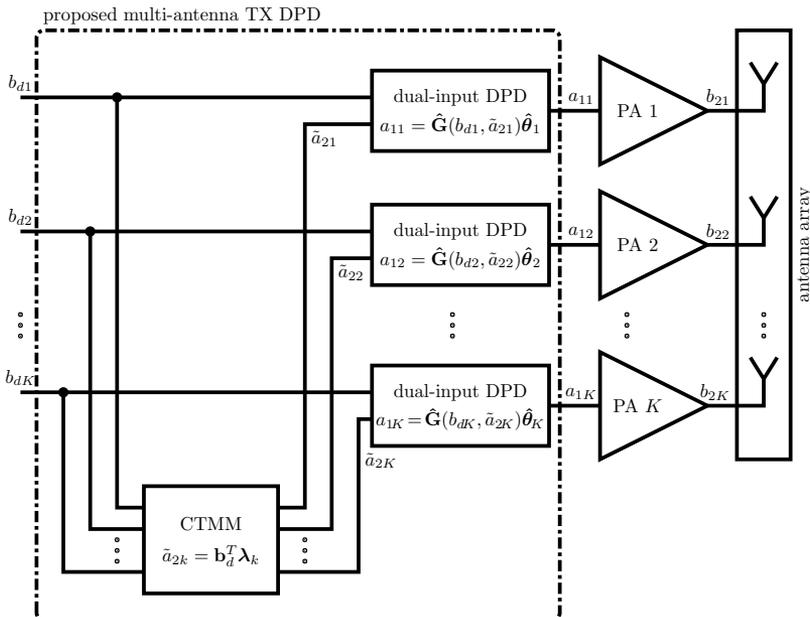
Figure 5.2. Block diagram of a multi-antenna transmitter with the proposed DPD method consisting of a linear CTMM block and dual-input DPDs.

The complexity of the CTMM for each transmit path increases linearly with the number of paths. The complexity of each dual-input DPD block is independent of the number of transmit paths. For transmitters with more than two paths, the complexity of the proposed DPD is lower compared to multi-input DPDs.

5.2 Identification of Predistorter Coefficients

Predistorter coefficients for multi-input structures and the proposed method can be found from measurements of the transmitter output signals. An alternative way of identifying the predistorter coefficients from over-the-air measurements is presented in Paper C. For the predistorter identification, the input signals to the different transmit path have to be different from each other and must not be fully correlated. However, for running the DPD no such restrictions apply.

5.2.1 From Measurements of Transmitter Output Signals

Multi-input DPD coefficients of the kth predistorter are identified from measurements of all transmitter output signals using least-squares estimation by

$$\hat{\boldsymbol{\theta}}_{k,LS} = \hat{\mathbf{G}} \left(\mathbf{b}_{21}, \ldots, \mathbf{b}_{2K} \right)^{+} \mathbf{a}_{1k}. \tag{5.4}$$

For the identification of the dual-input DPD coefficients, the CTMM coefficients have to be known. The CTMM coefficients can be identified using the method explained in Section 4.2.1, which is introduced in Paper B together with the DPD method. Another option is to identify the CTMM coefficients from S-parameter measurements as suggested in Paper A and explained in Section 4.2.2. Using the estimate $\tilde{a}_{2k}$ of the crosstalk signal, the dual-input DPD coeffcients of the kth predistorter are found by

$$\hat{\boldsymbol{\theta}}_{k,LS} = \hat{\mathbf{G}} \left(\mathbf{b}_{2k}, \tilde{\mathbf{a}}_{2k}\right)^{+} \mathbf{a}_{1k}. \tag{5.5}$$

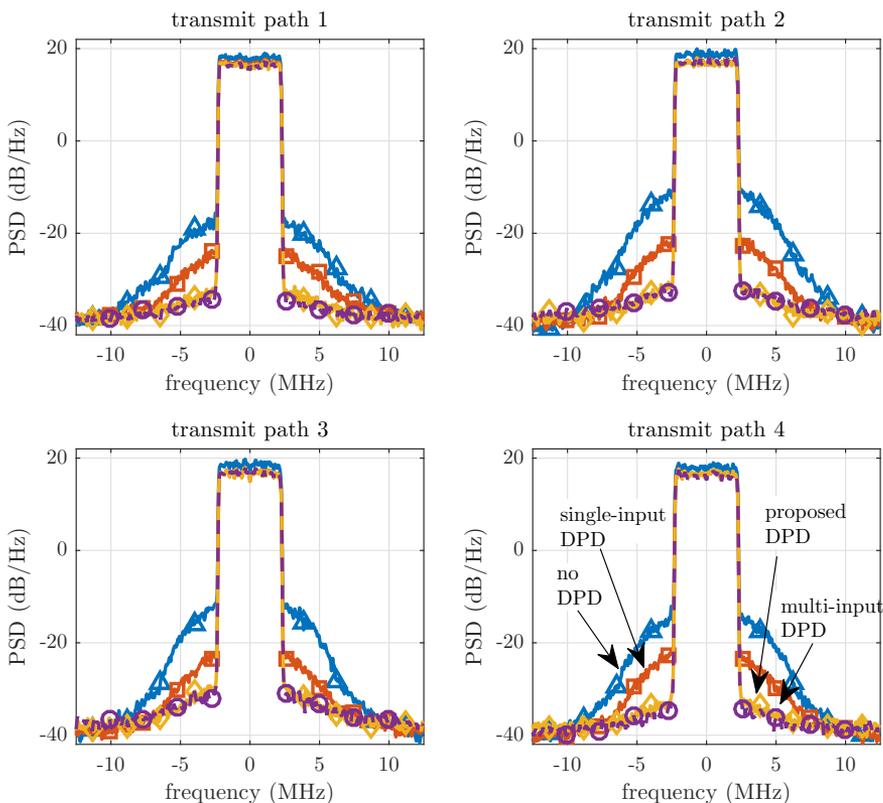**Figure 5.3.** Spectra of the transmitter output signals measured via couplers. The figure shows the results without DPD (blue △), with single-input DPD (red □), multi-input DPD (purple ○), and the proposed DPD (yellow ◇). The single input DPD does not consider the effects of crosstalk at all. The multi-input DPD and the proposed DPD are based on models using linear terms of the crosstalk signal.
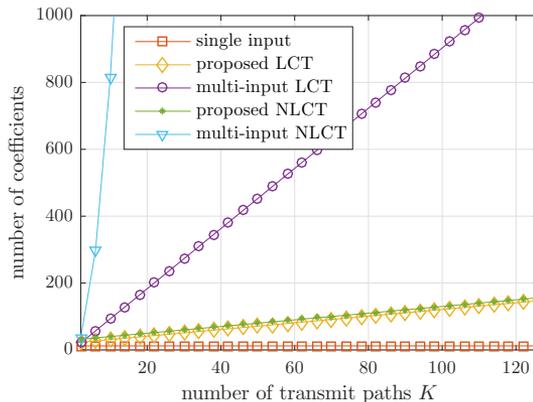
Figure 5.4. Illustration of how the number of coefficients per transmit path scales with the number of paths. The figure shows the number of DPD coefficients per switching region plus the number of CTMM coefficients. Numbers are shown for: single-input DPD; the proposed DPD and multi-input DPD based on models with linear crosstalk terms indicated by LCT; the proposed DPD and multi-input DPD based on models using linear and nonlinear terms of the crosstalk signals indicated by NLCT.

Experimental Results

The proposed DPD technique using the identification procedure from transmitter output signals was evaluated and compared to single-input and multi-input DPD techniques in measurements of a four-path transmitter. Also the CTMM was identified from the transmitter output signals, as described in Algorithm 4.2. The same transmitter as described in Section 4.2.1 was used. The bandwidth of the input signals was 5 MHz, and the sampling rate of the system was 25 MHz. Vector-switched [64] memory polynomial-based DPD structures were used for all DPDs. The PSDs of the individual transmitter output signals are shown in Figure 5.3. The multi-input DPD and the proposed DPD used for the results in the figure are based on model structures using only linear terms of the crosstalk signals. It can be seen in the figure that single-input DPD is not suitable to linearize the multi-antenna transmitter, since spectral regrowth is not eliminated sufficiently. The results for the proposed DPD technique and multi-input DPD reduce nonlinear distortion to a much lower level with approximately the same performance.

Figure 5.4, illustrates how the complexity of the different DPD techniques scales with the number of transmit paths. The complexity is evaluated based on the number of coefficients per transmit path per switching region. For the proposed DPD technique, the number of DPD coefficients includes the dual-input DPD coefficients and the CTMM coefficients. Numbers are given for model structures using linear and nonlinear terms of the crosstalk signals. For all multi-input DPDs, the number of coefficients increases rapidly with the number of transmit paths, while for the proposed DPDs only the number of

CTMM coefficients increases and the dual-input DPD is not affected. The numbers in the figure are specific to the transmitter used in the experiments. An exact prediction of the number of coefficients for other systems cannot be given. However, due to its structure, the proposed DPD technique will inherently have lower complexity than the multi-input DPD techniques for any transmitter where antenna crosstalk from more than one transmit path needs to be considered in the DPD.

5.2.2   From Over-the-Air Measurements

In a system implementation, measuring all transmitter output signals separately would require the use of one observation receiver per transmit path. However, equipping each transmit path with a dedicated observation receiver becomes expensive. Hence, in Paper C it is proposed to use MILA with over-the-air measurements to identify the predistorter coefficients. First, models of each individual transmit path are identified from over-the-air measurements with the procedure given in the paper, also explained in Section 4.2.3. The predistorter coefficients are then identified from the modeled transmitter output signals rather than the measured output signals. Based on modeled transmitter output signals $\tilde{b}_{2k}$, the predistorter coefficients are found by

$$\hat{\boldsymbol{\theta}}_{k,LS} = \hat{\mathbf{G}} \left(\tilde{\mathbf{b}}_{2k}, \tilde{\mathbf{a}}_{2k} \right)^{+} \mathbf{a}_{1k}. \tag{5.6}$$

While the PA model extraction was presented only for dual-input PA models, predistorters can be extracted for any of the predistorter structures given in this section.

Simulation Results

The proposed approach for identifying predistorters was evaluated in simulations, which were performed as described in Section 4.2.3, where an 8×8 array was simulated. The bandwidth of the input signals was 5 MHz, and the sampling rate of the system was 25 MHz.

First, it was investigating whether the proposed model-based predistortion can reach similar linearization results as predistortion identified directly from individual transmit path outputs. Hence, predistorters identified from over-the-air measurements were compared to predistorters identified from the individually observed transmitter output signals. For both predistorter structures, the proposed method with dual-input DPDs and CTMM was used. The CTMM was assumed to be known, and therefore did not need to be identified separately. Sixty-two transmit paths were simulated. The SNR at the over-the-air observation receivers was assumed to be ideal, i.e., $\mathbf{w} = \mathbf{0}$. The number of samples was $N = 12500$. Results are shown in Figure 5.6, where NMSEs are given in the top row, and ACPRs in the bottom row. In Figure 5.6a results for a system without any DPD are given, in Figure 5.6b results for

predistorters identified from individually observed transmitter output signals are shown, and in Figure 5.6c the results for predistorters found from observations of two over-the-air receivers are given. The predistorters identified from over-the-air measurements perform equally well as the predistorters extracted from measurements of all individual transmitter output signals.

The performance of the proposed DPD extracted from over-the-air measurements was evaluated for low receiver SNRs. For low SNRs it can be necessary to increase the number of observation receivers or the number of observed samples N. An example is shown in Figure 5.5, where NMSEs and ACPRs are given for 40 dB receiver SNR. In Figure 5.5a, four observation receivers were used with $N = 12500$. In Figure 5.5b, two observation receivers were used with $N = 375000$ observed samples to obtain similar results. These results show that it is indeed possible to linearize every individual output signal of a multi-antenna transmitter using measurements from only few over-the-air observation receivers even for low receiver SNRs.

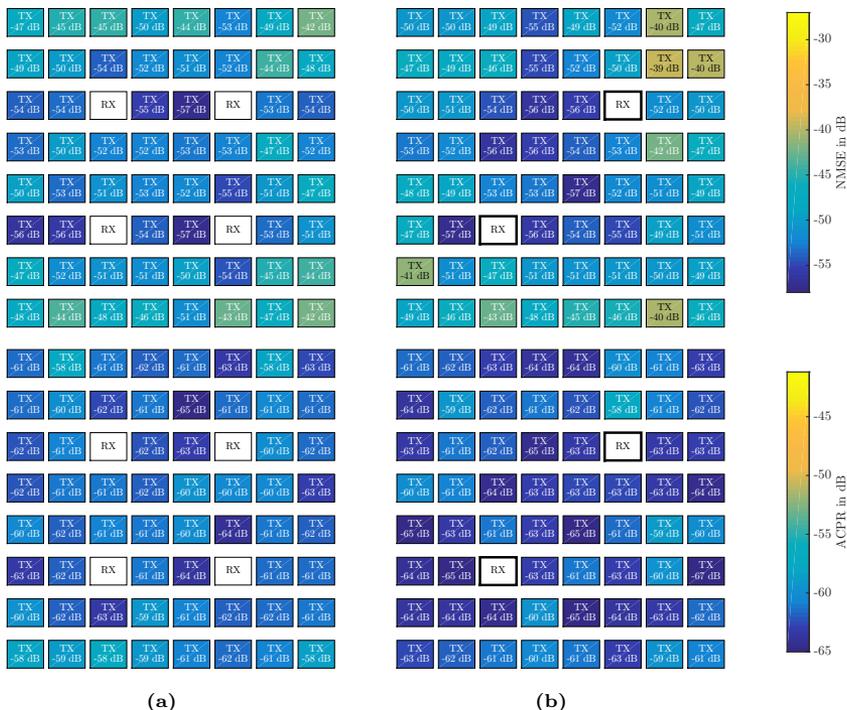**Figure 5.5.** NMSEs (top) and ACPRs (bottom) for DPDs extracted from over-the-air measurements for an 8×8 array with 40 dB receiver SNR: (a) four observation receivers, sixty transmit paths and $N = 12500$; (b) two observation receivers, sixty-two transmit paths and $N = 375000$. The position of receiver antennas is indicated by RX, and the position of transmitter antennas is indicated by TX.
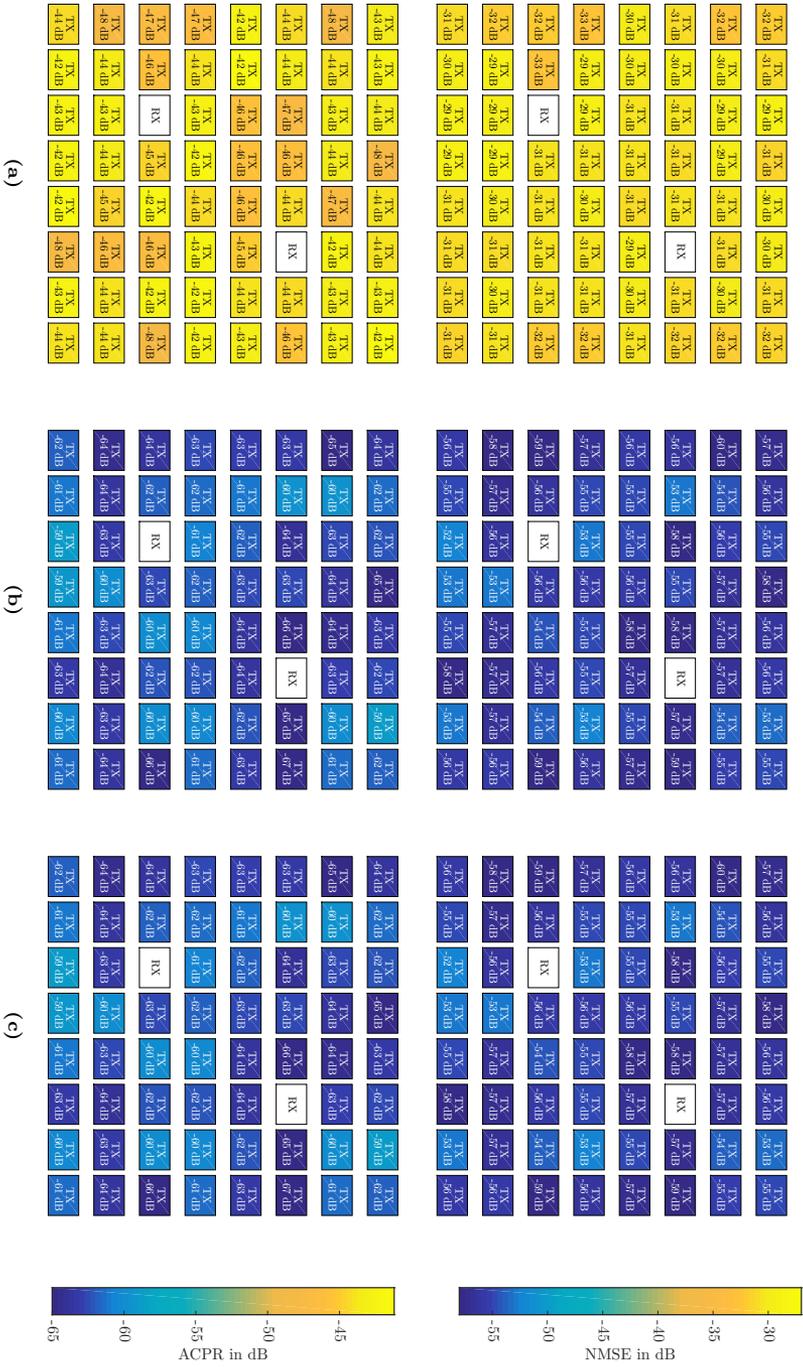
Figure 5.6. NMSEs (top) and ACPRs (bottom) with ideal receiver SNR with $N = 12500$ samples for every individual transmit path for the 8×8 array for: (a) no DPD, (b) DPD identified from individual observations of all transmit path outputs, (c) DPD with identification from observations of two over-the-air receivers, indicated by RX. Sixty-two antennas were connected to transmitters, indicated by TX. The results for DPD with conventional identification and the DPD with the proposed identification are the same.

Chapter 6

Conclusions and Future Work

6.1 Conclusions

Many challenges are faced in the design of multi-antenna transmitters. Due to the increasing number of antennas and transmit paths, transmit systems as well as their design process, are becoming more complicated and expensive. Therefore, complexity in terms of analog and digital hardware is a major concern. Transmitter hardware designs aim to avoid expensive and bulky components. However, this can lead to undesired effects that are not present in conventional single-path systems. Analysis and evaluation of transmitter performance in measurements become cumbersome and require expensive equipment, which makes it difficult to study and predict these effects.

In Paper A, a technique is presented that can predict the output of a multi-antenna transmitter of arbitrary size. The technique is based on dual-input PA models and models of antenna arrays. All models can be identified from individual measurements or simulations of the hardware components, such that a full transmitter implementation is not necessary for the implementation of the proposed technique. The technique can therefore be used for performance evaluation at an early design stage, for example, to compare combinations of different hardware components. This can help to save time and cost during the design process. The technique is also useful for developing and testing algorithms, like DPD, offline without conducting expensive and time-consuming measurements.

The digital predistortion technique presented in Paper B is designed to compensate for undesired effects due to nonlinear amplification, as well as crosstalk and mismatch. For large multi-antenna transmitters, the complexity of the technique scales well compared to existing solutions, which are not feasible to implement. Thus, the proposed technique facilitates low-cost analog

hardware designs by eliminating nonlinear distortion that is introduced as a consequence of the design choice.

In Paper C a method is proposed that allows to extract models of the individual PAs of a system by measuring linear combinations of all output signals via a small set of over-the-air observation receivers. This is in contrast to conventional solutions, which require a dedicated observation receiver for every single PA. The proposed algorithm can have an enormous positive impact on analog hardware complexity.

All in all, the work in this thesis provides signal processing solutions that facilitate both design and implementation of multi-antenna transmitters in several ways. The introduced modeling and prediction technique assists the development of such systems by making the design process more efficient and less expensive. The presented identification and linearization algorithms help to reduce both digital and analog hardware complexity, which can lower cost and energy consumption. Hence the presented work contributes to the development of feasible and sustainable solutions for future wireless communication system.

6.2   Future Work

Several problems concerning modeling and linearization of multi-antenna transmitters are still unsolved and could therefore be addressed in future work on the topic.

The technique presented in Paper A is limited to transmitters suffering from antenna crosstalk with relatively low levels of power. Hence, this work could be extended in order to make it suitable for transmitters suffering from higher crosstalk levels.

The linearization technique presented in Paper B only considers antennas that are wideband compared to the transmit signals. A useful continuation of the work presented in Paper B is to include dynamic antenna behavior such that it can be used for system with antennas that are narrowband compared to the signal bandwidth.

The theory presented in Paper C has only been confirmed in simulations. Measurement results should be used to ensure the usefulness of the approach. Furthermore, this work could be extended for cases where the crosstalk and channel coefficients are unknown.

References

[1] R. N. Clarke, "Expanding mobile wireless capacity: The challenges presented by technology and economics," *Telecommunications Policy*, vol. 38, no. 8, pp. 693 – 708, 2014. [Online]. Available: http://www.sciencedirect.com/science/article/pii/S0308596113001900

[2] 3rd Generation Partnership Project Technical Specification Group Radio Access Network, "Evolved Universal Terrestrial Radio Access (E-UTRA); Physical channels and modulation (Release 14)," Technical Specification 3GPP TS 36.211 V14.4.0 (2017-09), Sept 2017, 3GPP Organizational Partners (ARIB, ATIS, CCSA, ETSI, TSDSI, TTA, TTC), accessed on 2017-10-20. [Online]. Available: https://portal.3gpp.org/desktopmodules/Specifications/SpecificationDetails.aspx?specificationId=2425

[3] "5G Radio Access," Ericsson White Paper, Uen 284 23-3204 Rev C, April 2016, accessed on 2017-03-02. [Online]. Available: https://www.ericsson.com/res/docs/whitepapers/wp-5g.pdf

[4] F. Rusek, D. Persson, B. K. Lau, E. Larsson, T. Marzetta, O. Edfors, and F. Tufvesson, "Scaling up MIMO: Opportunities and challenges with very large arrays," *IEEE Signal Process. Mag.*, vol. 30, no. 1, pp. 40–60, Jan 2013.

[5] E. Costa and S. Pupolin, "M-QAM-OFDM system performance in the presence of a nonlinear amplifier and phase noise," *IEEE Trans. Commun.*, vol. 50, no. 3, pp. 462–472, March 2002.

[6] P. M. Lavrador, T. R. Cunha, P. M. Cabral, and J. C. Pedro, "The linearity-efficiency compromise," *IEEE Microw. Mag.*, vol. 11, no. 5, pp. 44–58, Aug 2010.

[7] M. Romier, A. Barka, H. Aubert, J.-P. Martinaud, and M. Soiron, "Load-pull effect on radiation characteristics of active antennas," *IEEE Antennas Wireless Propag. Lett.*, vol. 7, pp. 550–552, 2008.

[8] E. Ngoya and S. Mons, "Progress for behavioral challenges: A summary of time-domain behavioral modeling of RF and microwave subsystems," *IEEE Microw. Mag.*, vol. 15, no. 6, pp. 91–105, Sept 2014.

[9] L. Guan and A. Zhu, "Green communications: Digital predistortion for wideband RF power amplifiers," *IEEE Microw. Mag.*, vol. 15, no. 7, pp. 84–99, Nov 2014.

[10] A. Katz, J. Wood, and D. Chokola, "The evolution of PA linearization: From classic feedforward and feedback through analog and digital predistortion," *IEEE Microw. Mag.*, vol. 17, no. 2, pp. 32–40, Feb 2016.

[11] E. Larsson, O. Edfors, F. Tufvesson, and T. Marzetta, "Massive MIMO for next generation wireless systems," *IEEE Commun. Mag.*, vol. 52, no. 2, pp. 186–195, Feb 2014.

[12] L. Lu, G. Y. Li, A. L. Swindlehurst, A. Ashikhmin, and R. Zhang, "An overview of massive mimo: Benefits and challenges," *IEEE J. Sel. Topics Signal Process.*, vol. 8, no. 5, pp. 742–758, Oct 2014.

[13] F. M. Ghannouchi and O. Hammi, "Behavioral modeling and predistortion," *IEEE Microw. Mag.*, vol. 10, no. 7, pp. 52–64, Dec 2009.

[14] J. Kim and K. Konstantinou, "Digital predistortion of wideband signals based on power amplifier model with memory," *Electron. Lett.*, vol. 37, no. 23, pp. 1417–1418, Nov 2001.

[15] J. Pedro and S. Maas, "A comparative overview of microwave and wireless power-amplifier behavioral modeling approaches," *IEEE Trans. Microw. Theory Tech.*, vol. 53, no. 4, pp. 1150–1163, April 2005.

[16] J. Chani-Cahuana, P. N. Landin, C. Fager, and T. Eriksson, "Structured digital predistorter model derivation based on iterative learning control," in *European Microw. Conf.*, Oct 2016, pp. 178–181.

[17] A. Zhu and T. Brazil, "An overview of volterra series based behavioral modeling of RF/microwave power amplifiers," in *IEEE Annual Wireless and Microw. Technology Conf.*, 2006, pp. 1–5.

[18] M. Schetzen, *The Volterra and Wiener theories of nonlinear systems*, 2nd ed. Krieger Publishing Company, Malabar, Florida, 2006.

[19] D. Morgan, Z. Ma, J. Kim, M. Zierdt, and J. Pastalan, "A generalized memory polynomial model for digital predistortion of RF power amplifiers," *IEEE Trans. Signal Process.*, vol. 54, no. 10, pp. 3852–3860, Oct 2006.

[20] M. Isaksson, D. Wisell, and D. Rönnow, "A comparative analysis of behavioral models for RF power amplifiers," *IEEE Trans. Microw. Theory Tech.*, vol. 54, no. 1, pp. 348–359, Jan 2006.

[21] P. N. Landin, M. Isaksson, and P. Händel, "Parameter extraction and performance evaluation method for increased performance in RF power amplifier behavioral modeling," *International Journal of RF and Microwave Computer-Aided Engineering*, vol. 20, no. 2, pp. 200–208, 2010. [Online]. Available: http://dx.doi.org/10.1002/mmce.20422

[22] D. Zhou and V. DeBrunner, "A novel adaptive nonlinear predistorter based on the direct learning algorithm," in *IEEE Int. Conf. Commun.*, vol. 4, June 2004, pp. 2362–2366 Vol.4.

[23] C. Eun and E. J. Powers, "A new Volterra predistorter based on the indirect learning architecture," *IEEE Trans. Signal Process.*, vol. 45, no. 1, pp. 223–227, Jan 1997.

[24] P. N. Landin, A. E. Mayer, and T. Eriksson, "MILA - a noise mitigation technique for RF power amplifier linearization," in *IEEE Int. Multi-Conf. Syst., Sig. Devices*, Feb 2014, pp. 1–4.

[25] J. Chani-Cahuana, P. N. Landin, C. Fager, and T. Eriksson, "Iterative learning control for RF power amplifier linearization," *IEEE Trans. Microw. Theory Tech.*, vol. 64, no. 9, pp. 2778–2789, Sept 2016.

[26] J. Wood, "System-level design considerations for digital pre-distortion of wireless base station transmitters," *IEEE Trans. Microw. Theory Tech.*, vol. 65, no. 5, pp. 1880–1890, May 2017.

[27] J. Chani-Cahuana, C. Fager, and T. Eriksson, "A new variant of the indirect learning architecture for the linearization of power amplifiers," in *European Microw. Conf.*, Sept 2015, pp. 1295–1298.

[28] S. Amin, E. Zenteno, P. N. Landin, D. Rönnow, M. Isaksson, and P. Hndel, "Noise impact on the identification of digital predistorter parameters in the indirect learning architecture," in *Swedish Commun. Techn. Workshop*, Oct 2012, pp. 36–39.

[29] A. Tehrani, H. Cao, S. Afsardoost, T. Eriksson, M. Isaksson, and C. Fager, "A comparative analysis of the complexity/accuracy tradeoff in power amplifier behavioral models," *IEEE Trans. Microw. Theory Tech.*, vol. 58, no. 6, pp. 1510–1520, June 2010.

[30] L. Guan and A. Zhu, "Optimized low-complexity implementation of least squares based model extraction for digital predistortion of RF power amplifiers," *IEEE Trans. Microw. Theory Tech.*, vol. 60, no. 3, pp. 594–603, March 2012.

[31] P. M. Suryasarman and A. Springer, "A comparative analysis of adaptive digital predistortion algorithms for multiple antenna transmitters," *IEEE Trans. Circuits Syst. I*, vol. 62, no. 5, pp. 1412–1420, May 2015.

[32] A. Zhu, J. Pedro, and T. Brazil, "Dynamic deviation reduction-based Volterra behavioral modeling of RF power amplifiers," *IEEE Trans. Microw. Theory Tech.*, vol. 54, no. 12, pp. 4323–4332, Dec 2006.

[33] Y. Ma, Y. Yamao, Y. Akaiwa, and C. Yu, "FPGA implementation of adaptive digital predistorter with fast convergence rate and low complexity for multi-channel transmitters," *IEEE Trans. Microw. Theory Tech.*, vol. 61, no. 11, pp. 3961–3973, Nov 2013.

[34] A. Abdelhafiz, L. Behjat, F. M. Ghannouchi, M. Helaoui, and O. Hammi, "A high-performance complexity reduced behavioral model and digital predistorter for MIMO systems with crosstalk," *IEEE Trans. Commun.*, vol. 64, no. 5, pp. 1996–2004, May 2016.

[35] E. Zenteno, S. Amin, M. Isaksson, D. Rönnow, and P. Händel, "Combating the dimensionality of nonlinear MIMO amplifier predistortion by basis pursuit," in *European Microw. Conf.*, Oct 2014, pp. 833–836.

[36] N. Kelly and A. Zhu, "Low-complexity stochastic optimization-based model extraction for digital predistortion of RF power amplifiers," *IEEE Trans. Microw. Theory Tech.*, vol. 64, no. 5, pp. 1373–1382, May 2016.

[37] Z. Wang, W. Chen, G. Su, F. M. Ghannouchi, Z. Feng, and Y. Liu, "Low computational complexity digital predistortion based on direct learning with covariance matrix," *IEEE Trans. Microw. Theory Tech.*, vol. PP, no. 99, pp. 1–11, 2017.

[38] K. Iniewski, *Wireless Technologies Circuits, Systems, and Devices.* CRC Press, Taylor & Francis Group, LLC, 2008.

[39] T. Sadeghpour, R. Alhameed, N. Ali, I. T. E. Elfergani, Y. Dama, and O. Anoh, "Linear and nonlinear crosstalk in MIMO OFDM transceivers," in *IEEE Int. Conf. Electronics, Circuits Syst.*, 2011, pp. 504–507.

[40] D. Saffar, N. Boulejfen, F. M. Ghannouchi, A. Gharsallah, and M. Helaoui, "Behavioral modeling of MIMO nonlinear systems with multivariable polynomials," *IEEE Trans. Microw. Theory Tech.*, vol. 59, no. 11, pp. 2994–3003, Nov 2011.

[41] S. Bassam, M. Helaoui, and F. Ghannouchi, "Crossover digital predistorter for the compensation of crosstalk and nonlinearity in MIMO transmitters," *IEEE Trans. Microw. Theory Tech.*, vol. 57, no. 5, pp. 1119–1128, May 2009.

[42] M. Amiri, S. Bassam, M. Helaoui, and F. Ghannouchi, "Matrix-based orthogonal polynomials for MIMO transmitter linearization," in *IEEE Int. Workshop Computer Aided Modeling, Analysis Design Commun. Links Networks*, 2010, pp. 57–60.

[43] S. Amin, P. Landin, P. Händel, and D. Rönnow, "Behavioral modeling and linearization of crosstalk and memory effects in RF MIMO transmitters," *IEEE Trans. Microw. Theory Tech.*, vol. 62, no. 4, pp. 810–823, April 2014.

[44] Z. A. Khan, E. Zenteno, P. Händel, and M. Isaksson, "Digital predistortion for joint mitigation of I/Q imbalance and MIMO power amplifier distortion," *IEEE Trans. Microw. Theory Tech.*, vol. 65, no. 1, pp. 322–333, Jan 2017.

[45] P. Suryasarman, M. Hoflehner, and A. Springer, "Digital pre-distortion for multiple antenna transmitters," in *European Microw. Conf.*, Oct 2013, pp. 412–415.

[46] P. Suryasarman and A. Springer, "Adaptive digital pre-distortion for multiple antenna transmitters," in *2013 IEEE Global Conf. Signal Information Process.*, Dec 2013, pp. 1146–1149.

[47] Z. Zhang, Y. Shen, S. Shao, W. Pan, and Y. Tang, "An improved cross talk cancelling digital predistortion for MIMO transmitters," *Mobile Information Systems*, vol. 2016, Article ID 5626495, 2016.

[48] C. Fager, X. Bland, K. Hausmair, J. Cahuana, and T. Eriksson, "Prediction of smart antenna transmitter characteristics using a new behavioral modeling approach," in *IEEE Int. Microw. Symp.*, June 2014, pp. 1–4.

[49] D. Root, J. Verspecht, D. Sharrit, J. Wood, and A. Cognata, "Broadband poly-harmonic distortion (PHD) behavioral models from fast automated simulations and large-signal vectorial network measurements," *IEEE Trans. Microw. Theory Tech.*, vol. 53, no. 11, pp. 3656–3664, Nov 2005.

[50] G. El Nashef, F. Torres, S. Mons, T. Reveyrand, T. Monediere, E. Ngoya, and R. Quere, "EM/circuit mixed simulation technique for an active antenna," *IEEE Antennas Wireless Propag. Lett.*, vol. 10, pp. 354–357, May 2011.

[51] G. Z. El Nashef, F. Torres, S. Mons, T. Reveyrand, T. Monediere, E. N'Goya, and R. Quere, "Second order extension of power amplifiers behavioral models for accuracy improvements," in *European Microw. Conf.*, Sept 2010, pp. 1030–1033.

[52] J. Cai, J. B. King, and T. J. Brazil, "An improved quadratic polyharmonic distortion behavioral model," *Int. Journal Microw. Wireless Techn.*, vol. 7, no. 6, p. 605613, 2015.

[53] H. Zargar, A. Banai, and J. Pedro, "A new double input-double output complex envelope amplifier behavioral model taking into account source

and load mismatch effects," *IEEE Trans. Microw. Theory Tech.*, vol. 63, no. 2, pp. 766–774, Feb 2015.

[54] J. Cai, R. Gonçalves, and J. C. Pedro, "A new complex envelope behavioral model for load mismatched power amplifiers," *Int. Journal RF Microw. Computer-Aided Engineering*, p. e21097, 2017. [Online]. Available: http://dx.doi.org/10.1002/mmce.21097

[55] F. M. Barradas, T. R. Cunha, and J. C. Pedro, "Digital predistortion of RF PAs for MIMO transmitters based on the equivalent load," in *Workshop Integr. Nonlinear Microw. Millimetre-Wave Circuits*, April 2017, pp. 1–4.

[56] Skyworks Solutions, Inc., "SKY66001-11: 2100 to 2200 MHz, +19 dBm Linear Power Amplifier," Data sheet, Nov 2013, accessed on 2018-01-08. [Online]. Available: http://www.skyworksinc.com/uploads/documents/ SKY66001_11_201936E.pdf

[57] H. Zargar, A. Banai, and J. C. Pedro, "DIDO behavioral model extraction setup using uncorrelated envelope signals," in *European Microw. Conf.*, Sept 2015, pp. 646–649.

[58] S. Gustafsson, M. Thorsell, and C. Fager, "A novel active load-pull system with multi-band capabilities," in *ARFTG Microw. Meas. Conf.*, 2013.

[59] C. Fager, K. Hausmair, T. Eriksson, and K. Buisman, "Analysis of thermal effects in active antenna array transmitters using a combined EM/circuit/thermal simulation technique," in *Workshop Integr. Nonlinear Microw. Millimetre-Wave Circuits*, Oct 2015, pp. 1–3.

[60] C. Fager, K. Hausmair, K. Buisman, K. Andersson, E. Sienkiewicz, and D. Gustafsson, "Analysis of nonlinear distortion in phased array transmitters," in *Workshop Integr. Nonlinear Microw. Millimetre-Wave Circuits*, April 2017, pp. 1–4.

[61] Y. Wang, J. Peng, Y. Li, K. X. Gao, , and X. Zeng, "A DPD system with multiple transmitter paths," Patent Application WO2 010 054 499 A1, May 20, 2010.

[62] S. Choi and E. R. Jeong, "Digital predistortion based on combined feedback in MIMO transmitters," *IEEE Commun. Lett.*, vol. 16, no. 10, pp. 1572–1575, Oct 2012.

[63] K. Hausmair, U. Gustavsson, C. Fager, and T. Eriksson, "Modeling and linearization of multi-antenna transmitters using over-the-air measurements," in *IEEE Int. Symp. Circuits Syst.*, May 2018, accepted for publication.

[64] S. Afsardoost, T. Eriksson, and C. Fager, "Digital predistortion using a vector-switched model," *IEEE Trans. Microw. Theory Tech.*, vol. 60, no. 4, pp. 1166–1174, April 2012.